# Effect of interfacial bonding on the structural and vibrational properties of InAs/GaSb superlattices

N. Herres, F. Fuchs, J. Schmitz, K. M. Pavlov, J. Wagner, J. D. Ralston,* and P. Koidl
*Fraunhofer-Institut für Angewandte Festkörperphysik, Tullastrasse 72, D-79108 Freiburg, Federal Republic of Germany*

C. Gadaleta and G. Scamarcio
*Dipartimento di Fisica, Gruppo Nazionale di Fisica Quantistica e Plasmi,*
*Universita' di Bari, via E. Orabona 4, I-70126 Bari, Italy*
(Received 4 December 1995)

We have studied InAs/GaSb superlattices (SL's) grown with either InSb-like or GaAs-like interfaces (IF's) on top of a GaSb buffer layer on (100) GaAs substrates. The InAs layer thickness was varied from 4 to 14 monolayers (ML) while the GaSb layer thickness was kept fixed at 10 ML. The type of IF bonds realized was verified by Raman scattering from mechanical IF modes. High-resolution x-ray diffraction using one- and two-dimensional mapping of symmetric and asymmetric reflections allowed us to determine independently the lattice parameters parallel and perpendicular to the growth direction. The GaSb buffer layer was found to be fully relaxed whereas the SL's with InSb-like IF's were coherently strained to the in-plane lattice parameter of the GaSb buffer for InAs layer thicknesses exceeding 6 ML. The strain distribution within the SL's with GaAs-like IF's was obtained from simulations of the x-ray reflection profiles. The SL's were found to be coherently strained close to the GaSb buffer and showed increasing strain relaxation with increasing distance from the buffer layer. In addition, these simulations provide an accurate determination of the SL periods. Well-resolved Raman spectra of backfolded longitudinal acoustic (LA) phonons were observed showing for SL's with InSb-like IF's folded LA phonon lines up to the seventh order. The spectrum of quasiconfined optical SL phonons was examined by Raman spectroscopy and by IR reflection. A detailed analysis of the IR reflection spectra allowed an independent determination of the individual layer widths within the SL stack, including the spatial extent of the GaAs-like IF mode. [S0163-1829(96)06820-8]

## I. INTRODUCTION

There is considerable current interest in InAs/GaSb superlattices (SL's) because of their broken-gap type-II band alignment with the conduction-band minimum of InAs lying below the valence-band maximum of GaSb. For sufficiently thin InAs and/or GaSb layers the sum of the quantization energies of electrons and holes exceeds the band overlap between the InAs conduction band and the GaSb valence band. As a consequence, a spatially indirect SL band gap opens between the topmost quantized hole state in the GaSb layers and the lowest confined electron level in the InAs layers. Thus, the SL band gap, which determines the infrared (IR) optical properties of InAs/GaSb SL's can be ''tuned'' through the entire mid- and far-IR spectral range by varying the individual layer thicknesses.[1] This property makes InAs/GaSb SL's interesting for applications in IR detectors[2] as well as in IR lasers.[3] Since there is no common anion or cation across the InAs/GaSb heterointerface, two types of interface bonds can be formed, either InSb- or GaAs-like. It has been shown that the band overlap at the InAs/GaSb heterojunction[4–6] as well as the IR absorption cutoff wavelength of InAs/GaSb SL's (Ref. 7), depend on the type of interface bond. In this study we focus on the effect of the two different types of interface (IF) bonds on the structural properties of InAs/GaSb SL's, as revealed by high-resolution x-ray diffractometry (HRXRD), Raman scattering, and FIR reflection.

HRXRD in general, and the recently developed technique of HRXRD space mapping in particular[8–10] are valuable tools for the structural analysis of semiconductor SL's. Structural parameters such as, e.g., the SL period and the average lattice parameters of the SL and, for heteroepitaxial growth, also the strain situation in the buffer layer and the SL stack, can be evaluated with high accuracy. For group III arsenide-antimonide SL's, it has been observed before that conventional rocking curve measurements very often yield relatively broad reflection profiles of the SL's.[11,12] The reason for the observation of such broad profiles is related to the materials properties and the measurement procedure, in particular to the open-ended detector conventionally used for so-called rocking curves. We addressed this problem by recording two-dimensional angular diffraction space maps.[8] By placing a narrow slit in front of the detector the ambiguity can be removed that diffracted intensity originating from several more or less extended peaks in reciprocal space enter the orifice of the detector at slightly different diffraction angles without being discriminated.

Raman spectroscopy has found widespread use for the study of vibrational modes in semiconductor SL's.[13] For InAs and GaSb the bulk phonon dispersions overlap since the combined atomic weights within the unit cells of InAs and GaSb are roughly the same. Thus, in an InAs/GaSb SL quasiconfined optical SL phonons are present, consisting of a set of extended and confined modes, the latter being localized in either the InAs or the GaSb layers. The change of both the group III and group V atoms at the InAs/GaSb heterointerface leads to the appearance of ''mechanical'' IF

 © 1996 The American Physical Society

modes due to the formation of chemical bonds across the interface not present in either of the two bulk materials.[14–18] These modes are sharply localized at the interface regions and lie either above the optical modes (GaAs-like IF) or in the gap between the optical and acoustic modes (InSb-like IF) of both InAs and GaSb. Raman scattering by IF modes allows a direct assessment of the type of IF bonds formed.[7,11,19] In addition to these optical modes, doublets of folded longitudinal acoustic (LA) phonon lines can be observed in SL's because of a backfolding of the acoustic phonon dispersion branches onto a reduced Brillouin zone given by the SL period.[13]

Recently, far-infrared (FIR) absorption and reflection spectroscopy have been used to study the optical phonon modes in InAs/AlSb heterostructures. From these experiments insight was gained into the structural properties of these heterostructures including the chemical bonding at the heterointerface, and the spatial extent of the interface region.[20–22] InAs/AlSb heterostructures as well as the present InAs/GaSb SL's can be grown heteroepitaxially on GaAs substrates using appropriate buffer layers.[7,20,23] The frequencies of the optical phonons of InAs, AlSb, and GaSb are well separated from the spectral region of the reststrahlen band of the GaAs substrate for which the sample is opaque. Therefore the optical density in the spectral region of the optical phonons of the constituents of, e.g., the InAs/GaSb SL is of the order of one. It has been shown that the frequency of the InAs transverse optical (TO) phonon in InAs/AlSb quantum-well structures depends on the elastic strain experienced by the InAs layers.[20] Evidence has been given that only the nondistorted regions of the InAs layers away from the heterointerfaces contribute to the TO phonon absorption line.[23] In addition, the width of the IF region can be extracted from the FIR data.

We report on a systematic investigation of the structural and vibrational properties of short period InAs/GaSb SL's, grown by molecular-beam epitaxy (MBE) with either InSb- or GaAs-like IF's. All SL's were in the semiconducting regime with a constant GaSb layer width of 10 ML and InAs layer widths ranging from 4 to 14 ML. For these layer thicknesses the effective SL band gap is expected to vary between 0.41 and 0.12 eV corresponding to the 3–12-$\mu$m wavelength range.[24]

The present paper is organized as follows. Section II gives a short description of the sample growth and of the various experimental techniques applied. In Sec. III the HRXRD data are presented and analyzed. Section IV covers the Raman spectroscopic results. The results of FIR reflection measurements are presented in Sec. V together with their quantitative analysis. Finally, a summary and the main conclusions are given in Sec. VI.

## II. EXPERIMENT

Samples were grown by solid-source MBE on undoped semi-insulating (100) GaAs substrates. Molecular beams of $Sb_2$ and $As_2$ were used. The $V_2$/III beam equivalent pressure ratio was between 1 and 2 for the growth of GaSb and 10–15 for the growth of InAs. Growth rates were in the range 0.8–1 $\mu$m/h. Sample growth started with a GaAs layer and a 10-nm-thick (2-ML GaAs)/(4-ML AlAs) SL. Then, a 100-nm-thick AlSb nucleation layer, an (8-ML GaSb)/(8-ML AlSb) smoothing SL, and a 1.1-$\mu$m-thick strain relaxed GaSb buffer layer were grown, followed by the 100-period InAs/GaSb SL (see Fig. 1). The InAs/GaSb SL was grown at 410 °C as measured by a thermocouple calibrated to a change in the surface reconstruction of GaSb. For further details on sample growth see Ref. 25. The InAs layer thickness was varied from 4 to 14 ML,[26] while the GaSb layer thickness was kept constant at 10 ML. In the following ($N$ ML InAs)/(10 ML GaSb) SL's will be designated as $N$/10 SL's. For each SL period pairs of SL's were grown with the shutter sequence for the growth of the interfaces chosen for the deposition of either 1-ML InSb or 1-ML GaAs. These shutter sequences resulted in the intended formation of either InSb- or GaAs-like interface bonds, as verified by Raman spectroscopy of IF modes (see Sec. III B).

| Layer | Thickness | Temperature |
|---|---|---|
| 100 periods undoped SL:<br>N ML InAs<br>10 ML GaSb | N=4,6,8,10,14 | 410 °C |
| undoped GaSb buffer | 11000 Å | 500 °C |
| (25 Å GaSb/ 25 Å AlSb)x10 SPSL | 500 Å | 530 °C |
| AlSb nucleation layer | 1000 Å | 570 °C |
| 4 ML AlAs (2ML GaAs-4 ML AlAs)x2 | 100 Å | 580 °C |
| GaAs layer | 1000 Å | 580 °C |
| GaAs substrate (semi insulating) | 500 μm | |

FIG. 1. Growth sequence of the present InAs/GaSb SL's grown with either InSb-like or GaAs-like IF's on (100) GaAs substrates using a thick strain relaxed GaSb buffer layer.

For HRXRD measurements we used a diffractometer as depicted in Fig. 2 equipped with a two-crystal four-reflection Ge beam conditioner[27] (220 reflection mode), a four-circle Eulerian cradle for sample and detector positioning, and a high-accuracy incremental encoder for accurate angle reading of the $\omega$ position (resolution 0.0001°, accuracy ±0.0003°).

With Cu $K\alpha_1$ radiation ($\lambda \approx 0.154\,06$ nm) originating from a line focus set perpendicular to the plane of dispersion, the dimension of the x-ray beam at the position of the center

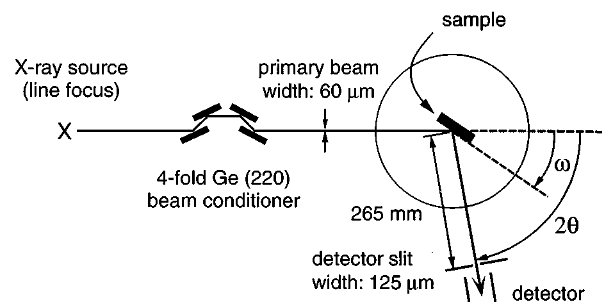


FIG. 2. High-resolution x-ray diffraction setup (dimensions given are within the plane of dispersion).

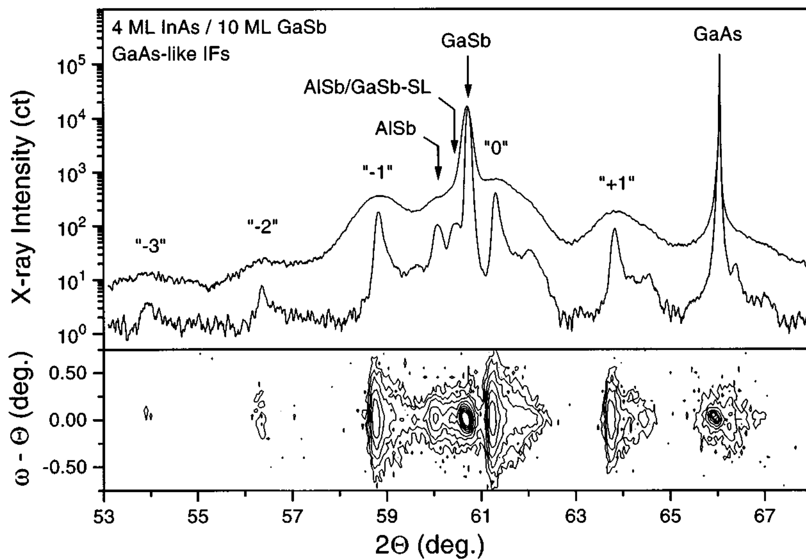


FIG. 3. One-dimensional (top) and two-dimensional (bottom) x-ray reflection profiles of a 4/10 SL with GaAs-like interfaces taken near the 004 reflections of GaAs(001) substrate and AlSb and GaSb buffer layers.

of the Eulerian cradle amounted to 0.06 mm×7.0 mm (width ×height). The samples were of 10 mm×10 mm size, their surface was positioned to within 0.03 mm of the cradle's center. We used an open detector (acceptance angle $\Delta 2\theta = 4°$) for low-resolution measurements.
In order to improve the signal-to-background ratio and to increase the angular resolution additional slit collimation on the detector side was used in a way similar to that shown by van der Sluis.[9] For high-resolution scans a 125 $\mu$m×10 mm slit in front of the detector resulted in an acceptance angle $\Delta 2\theta = 0.04°$. Two-dimensional reciprocal-space scans (angular space maps) were recorded using a 0.5-mm slit in front of the detector. This setting, tailored according to step sizes ($\Delta\omega/\Delta 2\theta$) used for the relatively large two-dimensional scans, corresponds to an acceptance angle $\Delta 2\theta = 0.12°$.

Prior to the measurements, the samples were aligned on a two-arc goniometer head inside the Eulerian cradle in such a way that the [001] direction of a specimen (i.e., the normal to the surface of the specimen) was set perpendicular to the vertical $\omega$ axis to better than 0.01°. In addition, using GaAs 444 asymmetric reflections, a [110] direction was adjusted parallel to the $\omega$ axis to better than 0.05°. By virtue of this aligning technique a Bond-type measurement procedure[28,29] was possible where all reflections belonging to the crystallographic zone in the plane of dispersion (i.e., perpendicular to both $\omega$ axis and a [110] direction of the specimen) are accessed subsequently by rotating the specimen around the $\omega$ axis only.

Tilts between substrate and film are thus easily checked for by comparing $00L$ reflection profiles taken at both sides ($-2\theta$ and $+2\theta$) of the primary x-ray beam. In order to establish the more or less strained lattice parameters of the substrate and the buffer layers we scanned subsequently the 002, 004, 006, 115− (grazing incidence), and 115+ (grazing exit) reflection ranges. With all sample movements done only around the $\omega$ axis (see Fig. 2), we can combine the readings from peak positions within the different reflecting ranges and then correct for refraction. In most cases we obtain the lattice parameters perpendicular and parallel to the plane of the specimen directly, i.e., without recurrence to an internal standard except for the wavelength used. For the refinement of the various structural parameters associated with the InAs/GaSb SL we made use of x-ray reflection profile simulations based on the dynamical theory of x-ray diffraction (Takagi-Taupin formalism[30]). In particular we used our own simulation program[31] and a simulation package provided by Siemens offering the important possibility to relax strained layers.[30,32]

Raman measurements were performed either at room temperature or at 77 K in backscattering geometry from the (100) growth surfaces. The spectra were excited with several lines of a Kr-ion and an Ar-ion laser. The laser light with a power of about 150 mW was focused to a spot size of 70 $\mu$m in diameter at the surface of the sample. For the InAs/GaSb SL's under study, the probing depth is 10–30 nm at room temperature for the present range of photon energies.[33] The scattered light was dispersed by a triple monochromator and detected with a liquid-nitrogen-cooled silicon charge-coupled device (CCD) detector array. The spectral resolution varied between 1 and 2.5 cm$^{-1}$.

Fourier-transform spectroscopy was used to measure the FIR reflectivity at spectral resolutions of 0.1–0.2 cm$^{-1}$ using a Ge bolometer for detection, operated at 2.3 K. The samples were mounted in a cold finger cryostat and cooled to 77 K. Samples were wedged to avoid interference fringes originating from the GaAs substrate.

## III. HIGH-RESOLUTION X-RAY DIFFRACTION

### A. Experimental x-ray reflection profiles

Figure 3 shows diffraction profiles of a 4/10 SL with GaAs-like interfaces taken by scanning in the $\Theta/2\Theta$ mode along the [001] direction in the 004 reflection range, using a fully open detector (upper curve) or a narrow slit in front of the detector (lower curve). On using the narrow detector slit, the resolution of the various diffraction peaks present in the x-ray reflection profiles improves considerably. Apart from the peaks attributable to the GaAs substrate, the AlSb and the GaSb buffer layers, several SL peaks (denoted by 0, ±1, ±2, etc.) are resolved in particular in the lower reflection profile. These peaks possess a shape consisting of a section with

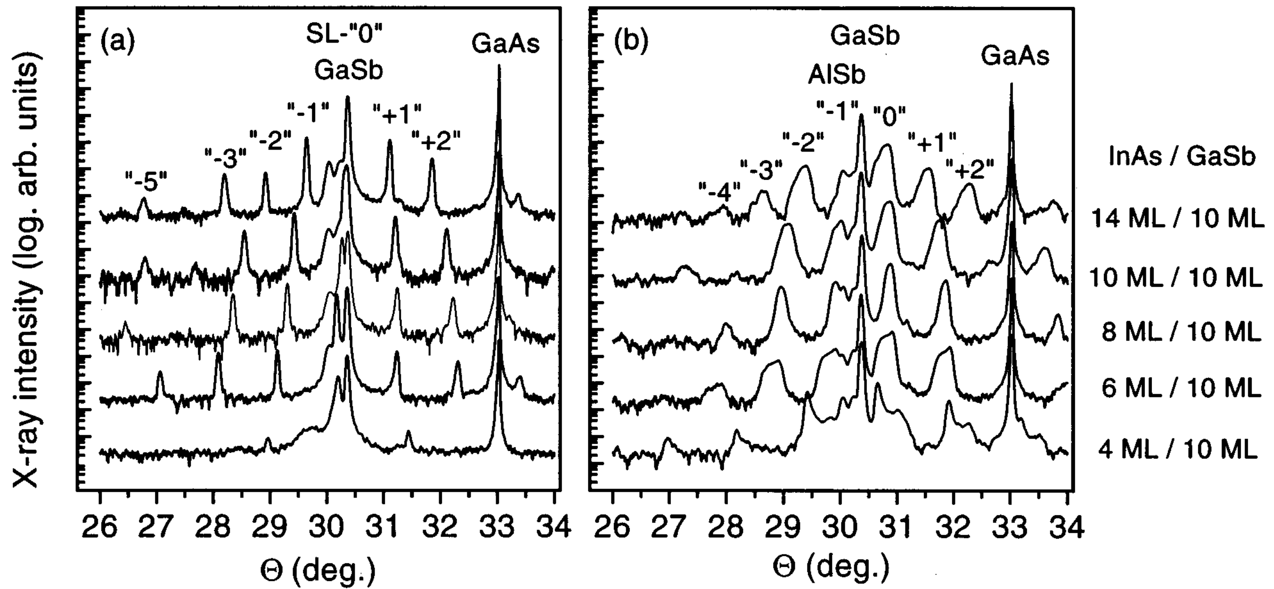


FIG. 4. X-ray reflection profiles (smoothed) near 004 fundamental reflections of $N/10$ SL's grown onto a GaSb buffer layer on (001) GaAs with (a) InSb-like interfaces and (b) GaAs-like interfaces.

high intensity at the low-angle side and a less intense shoulder extending to higher $\Theta$ values.

An even more detailed view of the situation is given in the two-dimensional angular diffraction space map in the lower part of Fig. 3. This angular space map is obtained by measuring several $\omega/2\Theta$ scans with different offsets $(\omega-\Theta)$, where $\omega$ denotes the angle between the sample surface and the incident beam, and $2\Theta$ the angle between incident and diffracted beams. We notice that the SL diffraction peaks show considerable broadening perpendicular to the median line, where $\omega=\Theta$ (i.e., a $\Theta/2\Theta$ scan). The intensity along this median line corresponds exactly to the better resolved $\Theta/2\Theta$ reflection profile displayed as the lower curve of the one-dimensional scans shown in Fig. 3. Reflection maxima originating from peaks of the substrate and the GaSb and AlSb buffer layers show nearly circular maxima on this map.

The largest broadening of the SL peaks in the angular space map is always found at the low-angle side $(2\Theta)$ of these peaks. At the high-angle side the SL peaks are confined to a region close to the median line. In order to explain this behavior we make use of a result presented later on. Some periods of this SL are strained to the in-plane lattice parameter of the GaSb buffer; these periods give rise to intensity collected at the high-angle part of SL peaks. However, most SL periods are either partly or fully relaxed, which results in a shift of the peak positions to lower angles and the considerable broadening observed perpendicular to the [001] direction.

Figure 4 shows x-ray reflection profiles near the 004 fundamental reflections for all samples investigated in this study recorded in the high-resolution $\Theta/2\Theta$ scan mode (i.e., with a 125-$\mu$m detector slit). From the SL lattice peaks assigned ''0'' the average lattice parameter $a_\perp$ perpendicular to the growth plane is obtained. For the samples with InSb-like interfaces the ''0'' peak of the SL's nearly coincides with the peak of the GaSb buffer layer in the case of the thicker InAs layers, i.e., the $a_\perp$ value for the SL nearly corresponds to that of the GaSb buffer. For SL's with InAs layer widths $\leqslant 6$ ML, however, the distinct shift of the SL peaks to lower angles shows that the $a_\perp$ values of the SL's are slightly larger than those of the GaSb buffer. For the samples with GaAs-like interfaces all SL peaks are somewhat less well defined. However, the position of the ''0'' peak on the high-angle side of the GaSb buffer peak indicates that here the $a_\perp$ values of the SL's are distinctly smaller than the $a_\perp$ values of the GaSb buffer. The broadening of the SL reflections observed with these samples is due to relaxation and will be discussed below.

In order to determine the lattice parameters $a_\parallel$ parallel to the growth plane and the strain situation within the SL from asymmetric reflections (e.g., 115), we have to resort to either two-dimensional reflection mapping or to one-dimensional reflection profiles taken with an open-ended detector. Figure 5 shows one- and two-dimensional reflection profiles in the angular range of the 115 fundamental reflections for a pair of 14/10 GaSb SL samples with either InSb-like or GaAs-like interfaces.

The measurement of angular space maps of asymmetric reflections is performed in much the same way as with symmetric reflections. In order to display a line of reference in such a map it is convenient to include an angle $\varphi$ in the description of the ordinate. In the present map this angle equals the angle between (001) and (115) planes in a cubic lattice and amounts to $\varphi=15.793°$. Thus we expect to find peaks belonging to unstrained cubic lattices along the line with $\omega-\Theta+\varphi=0$, which is the case for the GaAs substrate and the completely relaxed GaSb buffer layer. The SL peaks are found to be located along a slightly curved line (in reciprocal space these peaks are neatly aligned on a straight line), which intersects the line with $\omega-\Theta+\varphi=0$ near the GaSb peak at the position where we expect the ''0'' peak of the SL's (including knowledge from 004 reflection profiles).

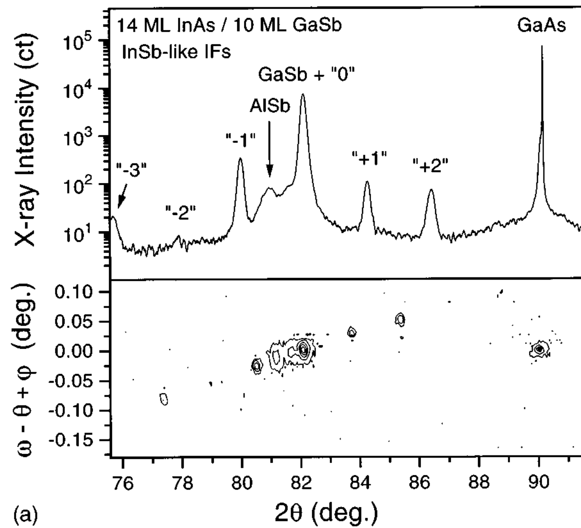


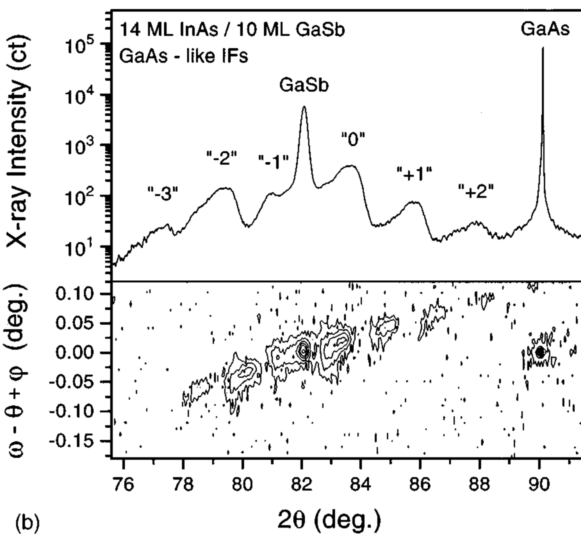


FIG. 5. One- and two-dimensional x-ray reflection profiles of two 14/10 SL's with (a) InSb-like interfaces and (b) GaAs-like interfaces.

Thus, both superlattices are elastically strained near to the cubic lattice constant of the GaSb layer. The better structural perfection of the SL with InSb-like IF's is evident from both one- and two-dimensional reflection profiles.

### B. Peak broadening mechanisms

In order to examine the present peak broadening, observed in particular for SL's with GaAs-like IF's, we may distinguish several possible mechanisms: tilting of different regions of the SL film, inhomogeneous strains, and a reduction of the size of reflecting crystallite domains within the SL film. Using the reciprocal lattice concept we can distinguish between these mechanisms (see Appendix A).

Prior to the evaluation of the measured reflection halfwidths one has to consider the experimental contributions from wavelength dispersion, beam divergence, beam width, and the acceptance angle of the detector.[34] In our case slit collimation on the detector side was very effective in improving the visibility of especially the SL peaks in $\Theta/2\Theta$ scans (Fig. 3). For the present SL's the broadening of the SL diffraction peaks is considerably larger perpendicular than parallel to the $\Theta/2\Theta$ scan direction (see Fig. 3). Thus, a cross talk between these two peak widths is negligible despite a detector acceptance angle of 150 arcsec. Therefore, for the present samples slit collimation is sufficient to evaluate the peak broadening of the GaSb and several InAs/GaSb SL reflections observed in $\omega$ scans. Assuming convoluted Gaussian contributions we reduced the observed full width at half maximum (FWHM) taking into account an experimental broadening of 40 to 120 arcsec depending on the Bragg angle $\theta$ and the measured FWHM encountered in the $\Theta/2\Theta$ scan of the same peak. This yielded reasonable values for the actual peak broadening because the instrumental contribution to the observed peak widths was always small.

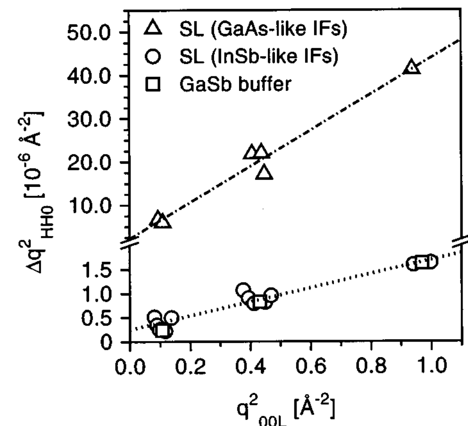


FIG. 6. Plots of $\Delta q^2$ vs $q^2$ for symmetric x-ray reflections $00L$ of the GaSb buffer (□) and the 4/10 SL (△) of a SL sample with GaAs-like IF's and the 14/10 SL of a SL sample with InSb-like IF's (○).

The broadening of the $00L$ reflections translated into reciprocal space are plotted in Fig. 6 as a function of the reciprocal lattice spacing of the corresponding $00L$ reflection [see Appendix A, Eq. (A4a)]. Data are shown for the GaSb buffer and the InAs/GaSb SL reflections of the 4/10 SL with GaAs like interfaces shown already in Fig. 3 and, for comparison, of a 14/10 SL with InSb-like IF's are also given in Fig. 6.

The evaluation of the data for the GaSb buffer shows that the ''crystallite size'' parallel to the surface, which is the size of coherently reflecting domains as obtained from the intercept with the ordinate, is $410\pm150$ nm. This value amounts to roughly $\frac{1}{2}$ of the total thickness of the GaSb layer. Mosaicity tilts constitute the major contribution of the broadening and amount to approximately $0.073\pm0.002°$, i.e., 0.04° with respect to the surface normal.

The InAs/GaSb SL of the same sample (Fig. 6) showed a significant amount of relaxation that is inhomogeneous across the SL stack. Therefore we performed $\omega$ scans at those $2\Theta$ positions where we encountered the strongest peaks (these positions coincide with the largest peak extensions in the angular space maps; see lower part of Fig. 3). The crystallite size parallel to the surface amounts to $94\pm44$ nm, which is about $\frac{1}{6}$ of the crystallite size in the GaSb buffer. Again mosaicity tilts constitute the major contribution to the broadening and amount to approximately 0.37

TABLE I. Materials parameters used for the modeling of x-ray reflection profiles.

| | $a_0$ (Å) | $c_{11}$ (GPa) | $c_{12}$ (GPa) | $\nu$ | $\alpha$ ($K^{-1}$) | Ref. |
|---|---|---|---|---|---|---|
| GaAs | 5.6536 | 119.00 | 54.00 | 0.312 | $6.0\times10^{-6}$ | 36, 37 |
| InAs | 6.0584 | 83.29 | 45.26 | 0.352 | $5.2\times10^{-6}$ | 35, 38 |
| GaSb | 6.0959 | 88.42 | 40.26 | 0.313 | $7.8\times10^{-6}$ | 35 |
| InSb | 6.4794 | 66.69 | 36.45 | 0.353 | $5.4\times10^{-6}$ | 35 |

$\pm0.02°$, i.e., $\pm0.18°$ with respect to the surface normal. We checked this finding by rotating around the diffraction vector prior to the $\omega$ scans and obtained the same FWHM with all azimuths (increment 15°) within the standard error (5%). In particular we did not find a difference with respect to the amount of the tilt around $\langle 110\rangle$ and $\langle 100\rangle$ directions for this sample.

The InAs/GaSb SL's of samples with InSb-like IF's are mostly elastically strained and yield sharp reflections. Figure 6 shows the effect of reflection broadening parallel to the surface for the 14/10 SL. The crystallite sizes parallel ($206\pm27$ nm) to the surface are about a factor of 2 smaller compared to those of the GaSb buffer layer. We tacitly assume that all GaSb buffer layers grown under the same conditions are similar with respect to the crystallite sizes. Mosaicity tilts constitute the major contribution of the broadening and amount to approximately $0.069\pm0.003°$ (i.e., $\pm0.035°$ with respect to the surface normal), which is nearly the same value as obtained with the GaSb buffer and a factor of 5 smaller compared to the 4/10 SL with GaAs-like IF's shown in Fig. 6.

### C. Determination of lattice parameters via profile fitting

In order to extract precise values for the structural parameters of the SL's, i.e., period $P_{SL}$ and lattice parameters $a_{\parallel}$ and $a_{\perp}$, from x-ray reflection data and gain additional information on the relaxation within the SL stack, we performed a full profile modeling of one-dimensional reflection profiles for the 002, 004, and 115 reflections of all samples.

The material parameters used in the simulation of x-ray reflection profiles are given in Table I.[35–38] For a description of the structures in terms of the number of layers of InAs, GaSb, InSb, and GaAs we used a procedure similar to that shown by Waterman *et al.*[7] We composed the SL of layers with a thickness of $\frac{1}{2}$ ML or $\frac{1}{4}$ of the elastically strained sphalerite lattice parameter of the respective binary compound. Unfortunately, the spatial resolution along the growth direction is lost to a certain extent, as our simulation programs need complete unit cells to calculate x-ray structure factors. Thus, to account for the IF regions we can either form mixed ternary or even quaternary compounds averaging over four layers or slice structure factors calculated from virtual complete unit cells. In either case, information regarding the phase of the structure factors is lost. In principle, this loss may influence relative peak intensities and can induce minute peak shifts.

Forming a mixed crystal perpendicular to the interface has the additional effect that alternating strains in adjacent layers may not be properly accounted for. At present, this problem cannot be resolved, as we are not aware of any simulation program where atomically thin layers can be handled correctly. Therefore, we do not expect to obtain always a full-profile fit with respect to peak intensities, and will have to be cautious to deduce compositional details ''inside'' the short period SL's from x-ray reflection profiles using these simulations. Fortunately, the program's ability to fit peak positions and thus extract SL periods and lattice parameters from x-ray reflection profiles is not affected by the problems described above, because this feature depends on the program's capability to handle crystal lattices, in the form of strained unit cells rather than crystal structures with emphasis on atomic positions and interatomic relationships.

The fitting procedure started by fixing the period $P_{SL}$ of a SL extracted from the spacing between SL peaks. Then, the location of the zero-order SL (''0'' SL) peak in symmetric reflection, which yields the average lattice parameter $a_{\perp}$ perpendicular to the growth plane, was determined combining data from 002, 004, and 006 reflection ranges. Next the position of the zero-order SL peak was fitted by adjusting the thicknesses of the differently strained InAs, GaSb, and interface layers within one SL period. In order to reduce the number of variables, we kept the number of GaSb bilayers in one series constant and fixed the width of the interface layers for all samples with the same type of interface. With the SL period given, the number of InAs bilayers is thus fixed for each sample. The remaining parameter representing the average degree of relaxation with respect to the GaSb buffer was adjusted until a reasonable fit of the peak positions in asymmetric reflections was obtained. In order to account for the observed peak widths for the SL's with GaAs-like interfaces we subdivided the 100-period SL's into units with the same degree of relaxation.

The determination of the structural parameters $P_{SL}$, $a_{\parallel}$, and $a_{\perp}$ and the modeling of strain profiles does not necessarily require a detailed knowledge of the chemical composition and the layer sequence within one SL period. However, in order to improve the fit of the x-ray diffraction profiles we decreased the width of the GaSb layers by 1 ML for SL's with InSb-like IF's and decreased the InAs layer width by 1 ML for both types with respect to the nominal values.

In addition we increased the IF width from 0.5 ML, corresponding to an ideally abrupt IF, to 0.75 ML for SL's with GaAs-like IF's. As both InAs and GaSb exhibit roughly the same monolayer thickness, their relative thicknesses can be modified without much impact on the overall strain. We obtained good profile fits for all samples with InSb-like and GaAs-like interfaces (see Figs. 7 and 8). In particular, the peak positions have been well reproduced. With respect to the peak intensities the agreement is less satisfying. Some of the peaks measured were near extinct in the simulations and vice versa (examples for these peaks can be found in Figs. 7

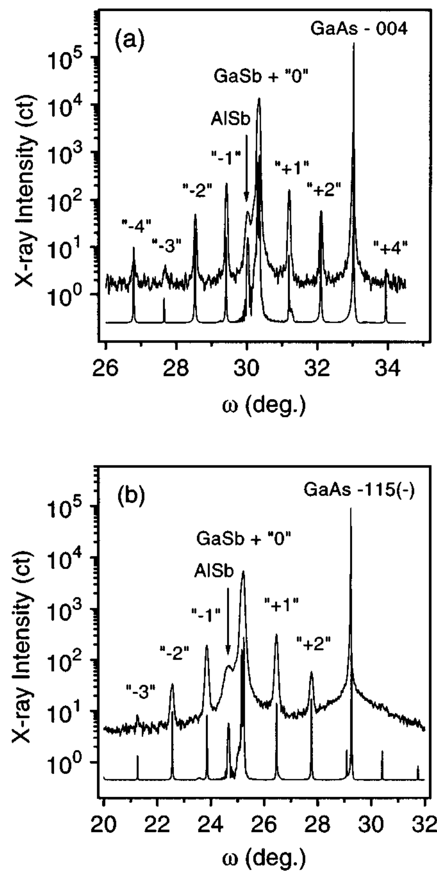


FIG. 7. Measured and simulated x-ray reflection profiles for a 10/10 SL with InSb-like interfaces covering (a) the 004 reflection range and (b) the 115(−) reflection range. The simulated profile has been smoothed with background added.

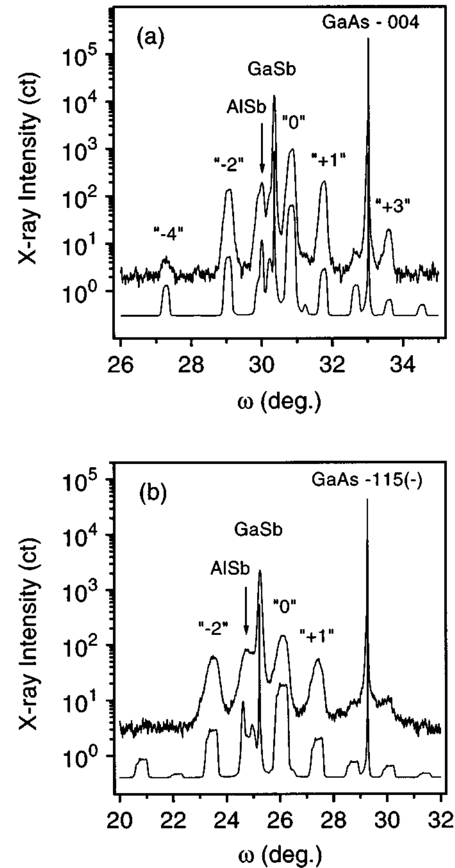


FIG. 8. Measured and simulated x-ray reflection profiles for a 10/10 SL with GaAs-like interfaces covering (a) 004 reflection range and (b) the 115(−) reflection range. The simulated profile has been smoothed with background added.

and 8). A possible reason for this has already been discussed and will be the subject of further study.

Table II lists refined values for the SL periods and the average lattice parameters of the InAs/GaSb SL's as determined from the above fits of the measured x-ray peak positions (confidence interval in parentheses). Comparing these values with those calculated on the basis of the nominal layer thicknesses, we find that the observed SL periods tend to be slightly smaller. We thus confirm similar observations by Waterman *et al.*[7] and Bennett *et al.*[39] The differences, however, are small and do not show a clear dependence on, e.g., the type of IF bonding. Thus the differences may be caused by statistical fluctuation of the SL period within the 100-period SL film. Judging from these data, we do not feel a necessity to discard the use of elastic deformations based on macroscopic elastic theory, even though this theory may be only an approximation when dealing with thin heavily strained layers.[4]

In Fig. 9 the variation of the average lattice parameters perpendicular [Fig. 9(a)] and parallel [Fig. 9(b)] to the growth direction is displayed for the two series of samples. In particular for all SL's grown with GaAs-like IF's we find that the average in-plane lattice parameter $a_{\parallel}$ is systematically smaller than that of the GaSb buffer layer, which indicates that these SL's are partially relaxed. For the SL's with InSb-like IF's, in contrast, only the 4/10 SL sample, i.e., that with the IF's closest to each other, shows some relaxation with the in-plane lattice parameter of the SL being larger than that of the GaSb buffer [Fig. 9(a)]. In agreement with earlier work by Bennett *et al.*[39] on InAs/GaSb SL's and Spitzer *et al.*[40] on InAs/AlSb SL's we find that samples with InSb-like interfaces are less prone to relax than samples with GaAs-like or nominally AlAs-like IF's. As reported by Lazzari *et al.*[41] the critical thickness of thick (AlGa)(AsSb) layers deposited on (001) GaSb depends on the direction of stress. For tensile strain the critical thickness amounts to roughly 20% of the thickness for which layers will start to relax under compressive strain. Our observations support this finding: SL's with GaAs-like IF's are under tensile strain and show stronger relaxation than SL's with InSb-like IF's, which are under compressive strain.

Reflection profiles for SL's with InSb-like IF's showed narrow reflection profiles (Fig. 7), which were fitted satisfactorily assuming a constant strain throughout each SL stack. For SL's with GaAs-like IF's, however, profile fitting of the considerably broadened SL peaks (Fig. 8) was only accomplished assuming a strain distribution. These strain profiles were constructed assuming a unidirectional strain distribution, with the portion of the SL stack closest to the GaSb buffer being coherently strained. Thus, for all SL's the in-plane lattice parameter $a_{\parallel}$ at the SL-buffer interface is that of the GaSb buffer with the lower part of all SL's being sub-

TABLE II. Intended and experimentally determined structural parameters of the $N/10$ SL's.

| Nominal SL sequence InAs/GaSb | IF type | SL period intended $P_{SL}$ (Å) | SL period observed $P_{SL}$ (Å) | Average lattice parameters of the SL intended $a_{\parallel}$ (Å) | intended $a_{\perp}$ (Å) | observed $a_{\parallel}$ (Å) | observed $a_{\perp}$ (Å) |
|---|---|---|---|---|---|---|---|
| 4/10 | InSb | 43.4 | 40.9 (2) | 6.096 | 6.136 | 6.117 (8) | 6.129 (6) |
| 6/10 | InSb | 49.4 | 48.4 (1) | 6.096 | 6.122 | 6.087 (6) | 6.131 (5) |
| 8/10 | InSb | 55.4 | 52.8 (1) | 6.096 | 6.110 | 6.095 (4) | 6.115 (3) |
| 10/10 | InSb | 61.5 | 57.3 (1) | 6.096 | 6.101 | 6.096 (4) | 6.107 (3) |
| 14/10 | InSb | 73.5 | 69.6 (1) | 6.096 | 6.087 | 6.090 (4) | 6.097 (3) |
| 4/10 | GaAs | 41.7 | 41.0 (3) | 6.096 | 6.014 | 6.044 (10) | 6.041 (8) |
| 6/10 | GaAs | 47.7 | 49.9 (9) | 6.096 | 6.014 | 6.070 (10) | 6.022 (8) |
| 8/10 | GaAs | 53.7 | 53.0 (3) | 6.096 | 6.014 | 6.081 (8) | 6.012 (6) |
| 10/10 | GaAs | 59.7 | 56.7 (3) | 6.096 | 6.015 | 6.075 (8) | 6.020 (6) |
| 14/10 | GaAs | 71.8 | 70.6 (2) | 6.096 | 6.015 | 6.074 (10) | 6.025 (8) |

jected to tensile strain. With increasing distance from the GaSb buffer the SL's relax. In the case of the thicker InAs layers (14/10; 10/10) the strain profiles are ''straight'' and nearly the same within the experimental uncertainty. Here the uppermost layers are relaxed to a state with very low strain. The strain profile of the sample with an ''intermediate'' thickness of the InAs layers (8/10) shows a ''straight'' behavior with some tensile strain left at the surface. The strain profile of the sample with the thinnest InAs layers (4/10) is different in two respects. First, complete relaxation is reached after approximately 30 periods. Second, the strain in the presumably upper half of the SL film is constant and compressive. We note that the average lattice parameters given in Fig. 9 for the samples with GaAs-like IF's are in fact the arithmetic averages of the position-dependent lattice parameters shown in Fig. 10.

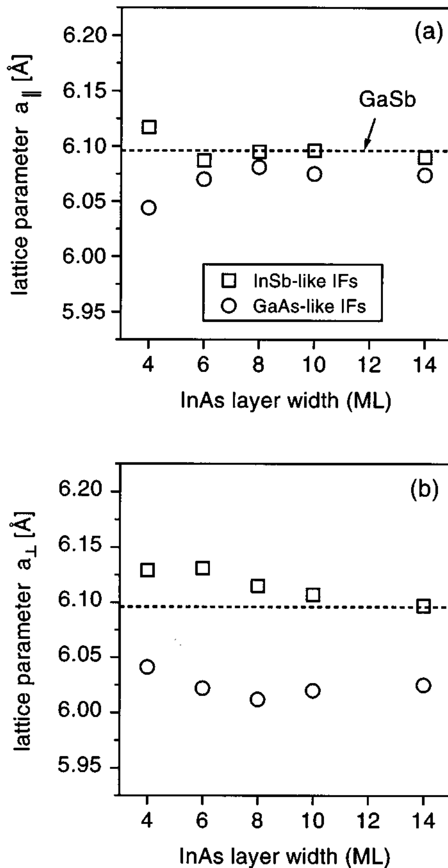


FIG. 9. Average lattice parameters of $N/10$ SL's with InSb-like IF's (□) or GaAs-like IF's (○) (a) parallel to the growth plane and (b) perpendicular to the growth plane.

A possible explanation for the very early relaxation observed in the SL with the thinnest InAs layers is the relative closeness of two highly strained interfaces, which promotes relaxation. We attribute the reduction of the strain towards the surface in the SL's with the thicker InAs layers to an increase in the number of dislocations. A similar observation has been made for the related system InAs/AlSb SL on (100)AlSb buffers by Spitzer *et al.*[40]

It is tempting to attribute the appearance of compressive strains in the uppermost part of some films (in particular those with 4- and 6-ML InAs and GaAs-like IF's) to the difference in the thermal expansion between substrate, buffer layers, and the SL films.[42] However, a calculation with room-temperature expansion data (Table I) in the present case shows that the amount of thermal strain that is expected with respect to the GaSb buffer ($\varepsilon_{therm} \approx -4 \times 10^{-4}$) on cooling down from growth temperature to room temperature is not sufficient to explain the observed amount of compressive strain in the upper part of the SL's with 4 and 6 InAs ML ($\varepsilon_{obs} = -2.5 \times 10^{-3}$ and $-1.2 \times 10^{-3}$), even if we assume that these SL portions might have been fully relaxed already at growth temperature.

## IV. RAMAN SPECTROSCOPY

Room-temperature Raman spectra covering the frequency range of the quasiconfined SL phonons and that of the zone-folded LA phonons are shown in Fig. 11 for a pair of 4/10 SL's with either GaAs- or InSb-like IF's. Besides the longitudinal optical SL phonons [LO(SL)] and the GaAs- and InSb-like IF modes at frequencies above and below the LO(SL) phonon line[7,11,19] well resolved and intense zone-folded LA phonon peaks[7,19,43] are observed for both types of IF bonds.

The dependence of the spectrum of IF modes on the intended type of IF bonds is shown more closely in Fig. 12.

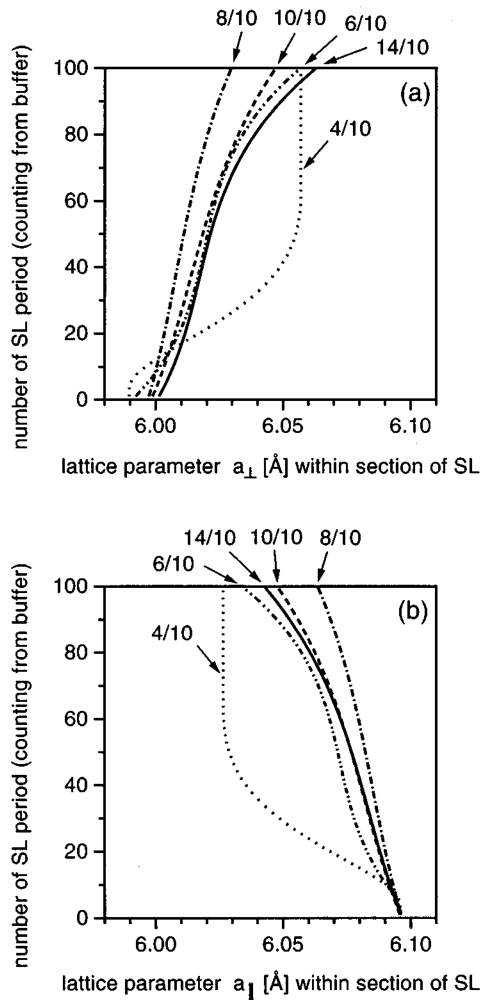


FIG. 10. Best-fit strain profiles extending through the $N/10$ SL's with GaAs-like IF's from the interface with the GaSb buffer to the surface of the SL; (a) strain perpendicular to the growth plane, and (b) strain parallel to the growth plane.

There, low-temperature spectra are plotted excited close to resonance with the 2.2-eV interband transition of the SL.[33] For the intended growth of Ga-As IF bonds the GaAs-like IF mode is the dominant feature in the spectrum. This mode occurs at a frequency of 256 $cm^{-1}$ for the strain relaxed 4/10 SL and at 254 $cm^{-1}$ for the 14/10 SL, which is coherently strained to the GaSb buffer. The observed IF mode frequencies indicate the formation of pure GaAs-like IF bonds with only a negligible admixture of Sb to the Ga-As IF layer.[44] The growth of the interfaces with a shutter sequence appropriate for the formation of In-Sb IF bonds results in a complete disappearance of the GaAs-like IF mode. Instead, an InSb-like IF mode appears at 190 $cm^{-1}$. This mode frequency is consistent with IF (InSb) mode frequencies of 192 and 194 $cm^{-1}$ reported in Refs. 7 and 43. The InSb-like IF mode is, in contrast, not detected for the SL grown with nominally GaAs-like IF bonds. The present Raman spectra clearly demonstrate that the growth of SL's with essentially pure GaAs-like or InSb-like IF's has been achieved. The spectral shape of the LO phonon band shows only a weak shoulder at frequencies above 240 $cm^{-1}$ for the case of InSb-like IF bonds, which indicates an unintentional incorporation

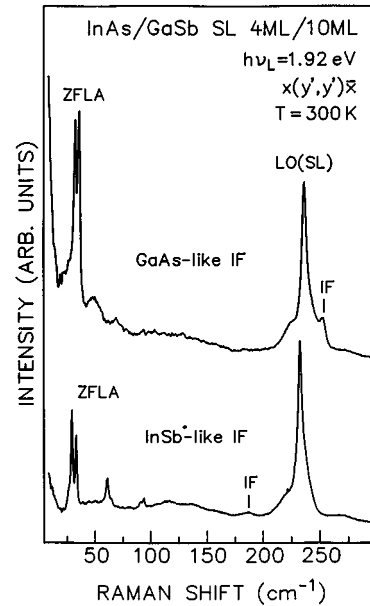


FIG. 11. Room-temperature Raman spectra of a pair of 4/10 SL's with (bottom) InSb-like and (top) GaAs-like IF's. Optical excitation was at 1.92 eV. Polarization of the incident and scattered light was parallel to the same (110) crystallographic direction $[x(y',y')\bar{x}]$.

of As into the GaSb layers at concentrations below 1%.[44]

Figure 13 shows room-temperature Raman spectra of SL's with GaAs-like IF's for InAs layer thicknesses of 4, 8, and 10 ML. The spectra were excited at 2.41 eV in between the 2.2- and 2.6-eV SL interband transitions[33] to minimize resonance effects. First, there is a systematic shift of the

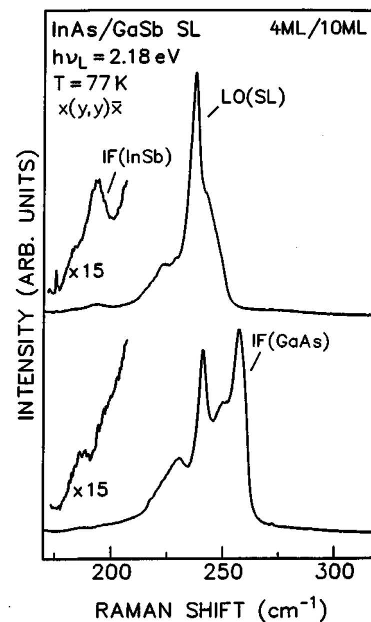


FIG. 12. Low-temperature (77 K) Raman spectra of a pair of 4/10 SL's with (top) InSb-like and (bottom) GaAs-like IF's. Optical excitation was at 2.18 eV. Polarization of the incident and scattered light was parallel to the same (100) crystallographic direction $[x(y,y)\bar{x}]$.

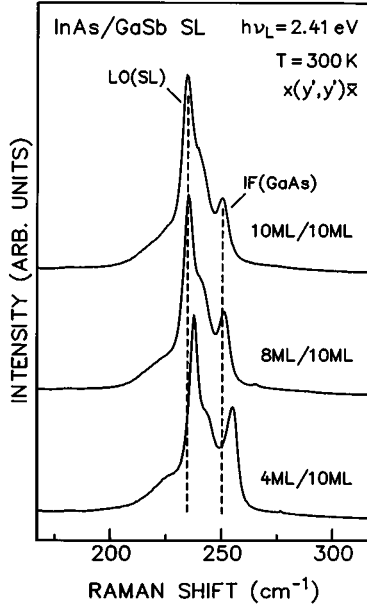


FIG. 13. Room-temperature Raman spectra of a set of $N/10$ SL's with GaAs-like IF's. The thickness $N$ of the InAs layers was varied from 4 to 10 ML. Optical excitation was at 2.41 eV. Polarization of the incident and scattered light was parallel to the same (110) crystallographic direction $[x(y',y')\bar{x}]$.

whole spectrum of SL phonons and the IF mode to higher frequencies with decreasing InAs layer width. Second, the relative strength of the GaAs-like IF mode increases with decreasing InAs layer thickness. The change in mode frequencies can be explained by variations in the elastic strain in the SL stack. For the 14/10 SL the average perpendicular strain $(a_\perp - a_\parallel/a_\perp)$ amounts to $-0.82\%$, whereas for the 4/10 SL the average strain is close to zero (see Fig. 9). The LO(SL) phonon band shifts to higher frequencies by 3 $cm^{-1}$ when going from the 14/10 SL to the 4/10 SL sample, corresponding to a shift of 3.7 $cm^{-1}$ per 1% perpendicular strain. For comparison, the strain-induced shift of the GaSb LO phonon has been found to be 3.3 $cm^{-1}$ per 1% strain[45] and that of the TO phonon in InAs has been determined to 2 $cm^{-1}$ per 1% strain.[20] Thus, the strain-induced frequency shift of the LO(SL) phonons is comparable to the frequency shifts reported for the optical phonons in the two bulk constituents InAs and GaSb.

Recently it has been shown that Raman scattering by the GaAs-like IF mode localized at the upper and lower IF appears in the $x(y',y')\bar{x}$ and $x(z',z')\bar{x}$ scattering configuration, where $x$, $y'$, and $z'$ denote ⟨100⟩, ⟨011⟩, and ⟨01−1⟩ crystallographic directions.[43] This finding has been explained by the orientation of the Ga-As IF bonds at the upper (GaSb on InAs) and the lower (InAs on GaSb) IF along two orthogonal ⟨110⟩-type directions.[43] An inequivalence of the upper and lower interfaces has been shown to result in differences in the Raman spectra recorded in the $x(y',y')\bar{x}$ and $x(z',z')\bar{x}$ scattering configurations.[43] For the present InAs/GaSb SL's room-temperature Raman spectra excited off resonance at 2.41 eV and recorded in the $x(y',y')\bar{x}$ and $x(z',z')\bar{x}$ configuration were identical with respect to both the SL phonons and the GaAs-like IF mode. This observation indicates that for the present set of samples the upper

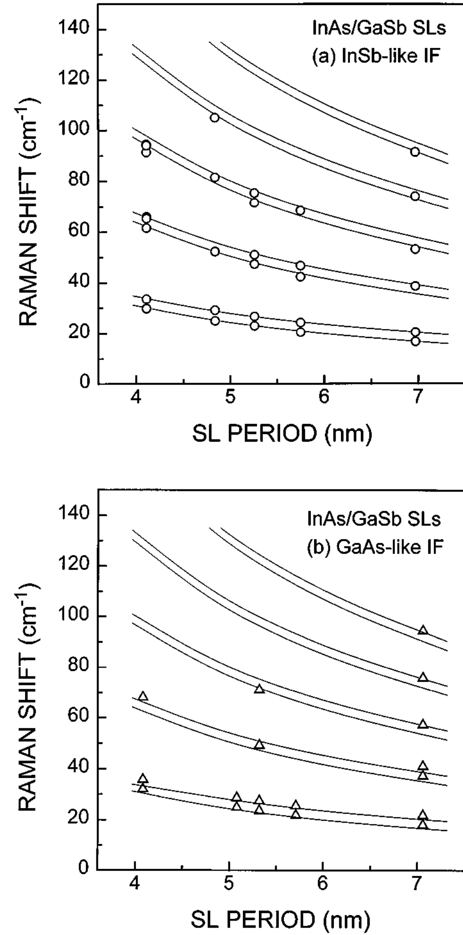


FIG. 14. Frequencies of zone-folded LA phonons in InAs/GaSb SL's with InSb-like IF's (a) and with GaAs-like (b) IF's vs the average SL period determined by HRXRD. Raman data were recorded for excitation at 1.92 eV. Full lines show calculated folded-mode frequencies.

and lower IF's are very similar in composition and spatial extent.[43]

Zone-folded LA phonon spectra were recorded from both series of InAs/GaSb SL's. The 14/10 SL's show folded LA phonons up to the seventh order for the sample with InSb-like IF's and up to at least the fifth order for the sample with GaAs-like IF's.[46] The observation of zone-folded acoustic phonons up to the seventh order underlines the high structural quality of the present InAs/GaSb SL samples with InSb-like IF's. The finding that zone-folded LA phonons are observed up to higher orders in SL's with InSb-like IF's than in SL's with GaAs-like IF's is consistent the observation of broader SL diffraction peaks in HRXRD for the latter than for the former type of SL's (see Sec. III).

In Fig. 14 the frequencies of the zone-folded LA phonon lines up to the fifth order are plotted versus the average SL period, determined by HRXRD, for InAs/GaSb SL's with InSb-like [Fig. 14(a)], and for SL's with GaAs-like IF's [Fig. 14(b)]. Also shown in Figs. 14(a) and 14(b) are calculated folded LA phonon frequencies as a function of the SL period $P_{SL}$. The calculations are based on the elastic continuum model with the frequency $\Omega$ of the $\pm m$th mode given by[13]

$$\Omega_{\pm m} = (m\pi/P_{SL} \pm \Delta k) v_{aver}. \quad (1)$$

Here $\Delta k$ is the momentum transferred in the backscattering experiment, which equals twice the momentum of the incident photon, and $v_{aver}$ is the averaged sound velocity of the SL given by $1/v_{aver}=\beta/v_{InAs}+(1-\beta)/v_{GaSb}$. $\beta$ is given by $d_{InAs}/P_{SL}$, where $d_{InAs}$ is the individual InAs layer thickness, and $v_{InAs}$ and $v_{GaSb}$ are the appropriate sound velocities of bulk InAs and bulk GaSb of $3.83\times10^5$ and $3.97\times10^5$ cm/s, respectively.[19] There is excellent agreement between the experimental data for the SL's with InSb-like lF's and the calculated curves in particular for the lower order doublets [see Fig. 14(a)]. This agreement demonstrates the consistency of the present Raman spectroscopic and HRXRD results regarding the period of the SL's under study.

However, for SL's with GaAs-like IF's the first-order folded LA phonon doublets occur at consistently higher frequencies than for SL's with InSb-like IF's. This becomes evident from Fig. 14(b) when comparing the experimental data points with the calculated folded LA phonon frequencies. According to Eq. (1) this frequency shift can be accounted for only by an increase in the average sound velocity for structures with GaAs-like IF's as the SL periods determined by HRXRD are very similar to both types of IF bonds (see Table II). Taking the frequencies of the first folded LA phonon doublets the relative change in the averaged sound velocity amounts to, e.g., 6.7% for the 14/10 SL. The present finding that the insertion of Ga-As IF bonds increases the average sound velocity is consistent with the sound velocity of bulk GaAs of $4.73\times10^5$ cm/s (Ref. 47), being significantly higher than the sound velocities in bulk InAs ($3.83\times10^5$ cm/s) and GaSb ($3.97\times10^5$ cm/s). A quantitative modeling of the average sound velocity including the GaAs-like IF's is complicated by the fact that the Ga-As IF bonds are highly strained and therefore it is questionable to represent these bonds by using the sound velocity of bulk GaAs. The corresponding sound velocity in InSb of $3.41\times10^5$ cm/s,[48] in contrast, differs much less from the sound velocities in bulk InAs and GaSb. Therefore, the zone-folded LA mode frequencies measured for SL's with InSb-like IF's can be explained by just taking a sound velocity averaged over the values for the two bulk constituents InAs and GaSb [see Fig. 14(a)].

## V. FIR REFLECTANCE

Figure 15 shows FIR reflectance spectra of a pair of 14/10 SL's grown with either InSb-like IF's (top) or GaAs-like IF's (bottom). The spectra are shifted vertically for clarity. In both spectra the TO phonon modes of all constituents of the SL are resolved as sharp features, well separated from the broad reststrahlen band of the GaAs substrate. The TO phonon modes of the InAs, GaSb, and AlSb are observed at 219, 230, and 340 cm$^{-1}$, respectively. The GaAs reststrahlen band extends over the range from 270 to 300 cm$^{-1}$. The InAs TO phonon line arises from the SL whereas the GaSb TO phonon band is a superposition of signals originating from the SL and from the 1.1-$\mu$m-thick GaSb buffer layer. The spectrum of the SL with GaAs-like IF's shows a spectrally sharp feature superimposed on the broad GaSb TO phonon band. The AlSb TO phonon mode stems from the AlSb nucleation layer placed underneath the GaSb buffer layer (see Sec. II and Fig. 1). Comparing the two spectra, besides the TO phonons of the individual constituents an additional broad band is observed at about 240 cm$^{-1}$ for the SL with GaAs-like IF's. This additional band is assigned to the GaAs-like IF mode, observed so far only by Raman spectroscopy[11,33] (see Sec. IV). Arsenic contamination in the GaSb SL layers leads to the appearance of a GaAs-like TO mode in that frequency range.[11] As such a contamination at the 1% level cannot be excluded from the Raman and x-ray measurements, a possible contribution from a GaAs-like TO mode cannot be excluded. However, the observed mode intensity is much higher than that expected for this TO mode.

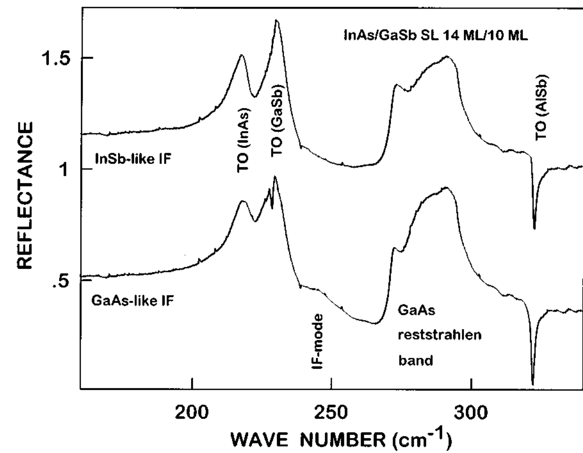


FIG. 15. FIR reflectance (normal incidence) of two 14/10 SL's with InSb-like and GaAs-like IF's.

The complete set of FIR reflectance spectra, covering the spectral range of the InAs and GaSb TO phonon modes, is shown in Fig. 16 for the two series of SL's. There is, independent of the type of IF bonds formed, a monotonic decrease in strength of the InAs TO phonon line with decreasing InAs layer thickness. All the spectra recorded from samples with GaAs-like IF's show the above-mentioned fea-

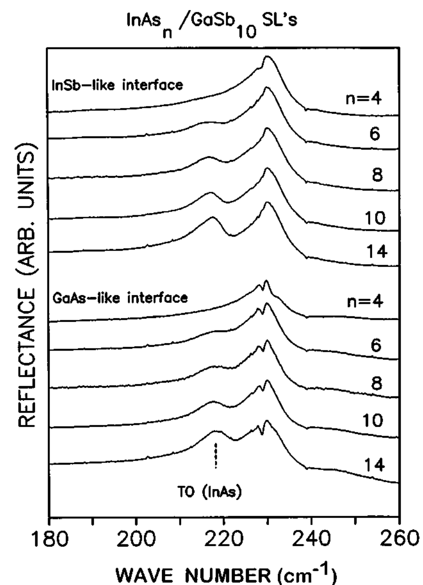


FIG. 16. FIR reflectance of two sets of samples, comprising $N$/10 SL's grown with InSb-like or GaAs-like interfaces. The InAs layer thickness $N$ has been varied from 4 to 14 ML.

TABLE III. Parameters used in the theoretical simulation of the FIR reflectance spectra.

| Layer type | Oscillation strength | Dielectric constant |
|---|---|---|
| GaSb | 1.25 | 14.4 |
| InAs | 2.9 | 12.25 |
| GaAs | 1.9 | 10.9 |
| AlSb | 1.8 | 10.24 |

ture superimposed on the GaSb TO phonon band.

The experimental spectra have been fitted by theoretical reflectivity curves obtained by calculating the transfer matrix of the propagation of the electromagnetic radiation in the whole stratified medium.[49] In order to best model the FIR reflectance spectra of the investigated samples, not only the reflectance of the SL but also that of the buffer layers and of the substrate have to be taken into account. The dielectric function $\epsilon_{SL}$ of the InAs/GaSb SL's has been described in the framework of the effective medium approximation (see Appendix B). To take into account the GaAs-like bonds at the interface of the SL's grown with those IF's, one SL period has been modeled by the following sequence of bilayers:

$$(\mathrm{InAs})_N(\mathrm{GaAs\text{-}IF})_{N''}(\mathrm{GaSb})_{M'}(\mathrm{GaAs\text{-}IF})_{M''}. \qquad (2)$$

The vibrational modes in the layers with thicknesses $N'$ and $M'$ are given by the InAs and GaSb TO phonon modes, respectively. Confinement effects, which result in a series of quasi-confined TO modes, are neglected. In the experiment only the superposition of these modes is resolved. Assuming a linear response these quasiconfined TO modes can be described by a single mode when an appropriate damping constant is chosen. Similarly, also variation of the GaSb TO phonon frequency caused by the nonuniform strain can be treated phenomenologically by using an averaged mode frequency with an increased linewidth. In order to fit the present data a phonon damping between 2 and 3 $\mathrm{cm}^{-1}$ has been chosen (see Appendix B). It will be shown below that the nonuniform strain observed by x-ray diffraction leads to shifts in the averaged phonon frequency of about 1 $\mathrm{cm}^{-1}$.

In the layers with thicknesses $N''$ and $M''$ an additional harmonic oscillator is introduced to represent the IF vibrational mode. The localization lengths of the GaAs-like IF are described by $N''$ and $M''$, respectively. The thicknesses $N$ and $M$ of the InAs and GaSb layers are given by $N=N'+N''$ and $M=M'+M''$, respectively. The GaSb layer thickness has been fixed at its nominal value of 10 ML. Due to the presence of the reststrahlen band of the GaSb buffer the actual GaSb layer thickness in the SL's could not be determined with sufficient accuracy from the experimental spectra. By fitting the experimental FIR reflectivity spectra we were able to determine the frequencies of the optical modes localized in each layer or at the interface of the SL, as well as extract the actual thickness of the InAs layers and the localization length of the IF mode, provided the oscillator strength of each mode is known (see Table III). In the case of GaAs-like IF layers, the damping factor $\Gamma$ has also been determined to 10 $\mathrm{cm}^{-1}$. For the InAs and GaSb TO phonons in the SL damping factors in the range 2–3 $\mathrm{cm}^{-}$ have been used. The other materials parameters (Table III), including those of the

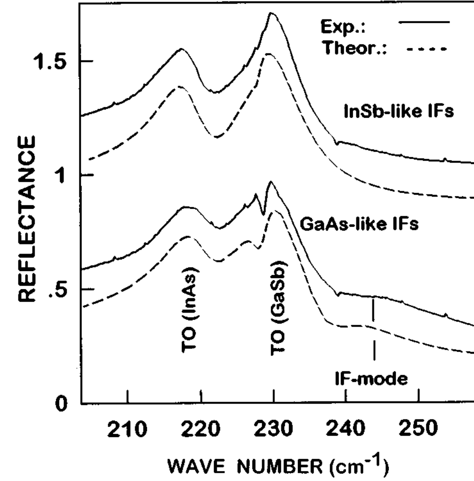


FIG. 17. Comparison between experimental (full lines) and calculated (dashed lines) FIR reflectance spectra of two 14/10 superlattices. Spectra have been offset for clarity. The two upper traces correspond to SL's grown with InSb-like IF's, the two lower curves refer to SL's with GaAs-like IF's. For SL's grown with GaAs-like IF's the contribution of the GaAs-like IF mode has been included in the calculation.

buffer layers and substrate, have been taken from Ref. 35. Further details of the calculation procedure are outlined in Appendix B.

In Fig. 17 experimental (full lines) and calculated (dashed lines) FIR reflectance spectra are shown for a pair of 14/10 SL's with different IF's. The spectra have been offset for clarity. The two upper traces correspond to the sample with InSb-like IF's, the two lower traces refer to the sample with GaAs-like IF's. For the latter sample the GaAs-like IF mode has been included in the calculation. The spectra are well reproduced by the calculations. From these fits we obtain the frequencies and intensities of the InAs and GaSb TO phonon modes. The quantitative evaluation of the intensities allowed us to deduce the thickness of the individual layers (Tables IV and V), while the frequencies provide insight into the strain situation of the layers.

Furthermore, information on the GaAs-like IF mode is gained. The frequency of this mode is determined to 242 $\mathrm{cm}^{-1}$. If we identify this vibrational mode with a transverse mode and assign the GaAs-like IF mode, observed by Raman spectroscopy at a frequency of 254 $\mathrm{cm}^{-1}$ for the present SL, in agreement with Ref. 14, to a longitudinal mode we can deduce the oscillator strength $a$ for this IF vibration to 1.25 using the well-known relation

TABLE IV. Results of the numerical evaluation of the FIR reflectance of the series of $N$/10 SL's grown with GaAs-like interfaces.

| Nominal comp. | Evaluated thickness (ML) | | Phonon energies ($\mathrm{cm}^{-1}$) | |
|---|---|---|---|---|
| InAs/GaSb (ML) | GaAs IF | InAs | InAs TO | GaSb TO |
| 4/10 | 3.9 | 0 | | 229 |
| 6/10 | 4.8 | 2.9 | 218.5 | 229 |
| 8/10 | 4.8 | 5.4 | 218.8 | 229 |
| 10/10 | 4.8 | 7.0 | 218.3 | 229 |
| 14/10 | 4.8 | 10.6 | 218.7 | 229 |

$$a=\varepsilon_0\,\frac{\omega_{\mathrm{LO}}^2-\omega_{\mathrm{TO}}^2}{\omega_{\mathrm{TO}}^2}\,. \tag{3}$$

With this value for the oscillator strength at hand we can give an estimate of the spatial extent of the eigenvectors of the IF mode along the growth direction.

Resulting values for the spatial extent of the GaAs-like IF mode along with the thicknesses of the InAs layers within the SL stack, also deduced from the modeling of the FIR reflectance spectra, are given in Tables IV and V for SL's with GaAs-like and InSb-like IF's, respectively. The estimated localization length of the GaAs-like IF mode of 2–3 ML is consistent with eigenvectors calculated for an ideal abrupt InAs/GaSb IF with GaAs-like interfacial bonding.[50] These calculations showed that, besides the Ga-As bilayer at the IF, also the two neighboring atomic planes in the InAs layer as well as those in the GaSb layer show a nonvanishing vibrational amplitude.[50]

The high spectral resolution of the Fourier transform measurements allows us to determine phonon frequencies within an accuracy of 0.1 $\mathrm{cm}^{-1}$. The InAs TO phonon frequencies obtained by fitting the FIR reflectance spectra are also listed in Tables IV and V for the SL samples with GaAs-like and InSb-like IF's, respectively. There is a significant difference between the InAs TO phonon frequencies found for SL's with GaAs-like IF's and those found for SL's with InSb-like IF's. The average frequency for the former type of IF bonds is 218.5 $\mathrm{cm}^{-1}$ and for the latter type of bonds 217.4 $\mathrm{cm}^{-1}$. The corresponding low-temperature value for unstrained bulk InAs is 220.5 $\mathrm{cm}^{-1}$.[51]

As discussed in detail in Sec. III the present InAs/GaSb SL's with InSb-like IF's are coherently strained to the in-plane lattice constant of the GaSb buffer for InAs layer thicknesses $N\geqslant 6$ ML, while the SL's grown with GaAs-like IF's show an increasing degree of relaxation with increasing layer thickness. Based on continuum elasticity theory the frequency of the InAs TO phonon is expected to be shifted by 1.3 $\mathrm{cm}^{-1}$ to lower values because of the biaxial in-plane tension to which the InAs layers are subjected in the case of coherent strain to the GaSb lattice constant.[13,52,53] This shift results in an expected value for the InAs TO phonon frequency in the present set of SL's of 219.2 $\mathrm{cm}^{-1}$. Thus there remains a difference of 1.8 $\mathrm{cm}^{-1}$ between this value and the experimentally determined frequency of the SL's grown with InSb-like IF's.

The remaining differences of 0.7 and 1.8 $\mathrm{cm}^{-1}$ for SL's with GaAs-like and InSb-like IF's between the expected value of 219.2 $\mathrm{cm}^{-1}$ and the frequencies deduced from the experiment cannot be accounted for by strain effects. Instead, as we deal with an InAs/GaSb SL with individual layer thicknesses of the order of 10 ML or even less, most likely phonon confinement effects of the order of 2 $\mathrm{cm}^{-1}$ have to be taken into account.[14,15,17,18]

The smaller redshift of only 0.7 $\mathrm{cm}^{-1}$ found for SL's with GaAs-like IF's can be explained by the partial relaxation of the SL observed with HRXRD at this sample series. As shown in Sec. III the in-plane lattice parameter of the samples grown with GaAs-like IF bonds decreases with increasing distance from the value of the GaSb buffer to approximately the value of InAs. Therefore the strain-induced redshift can only be expected for the first 20 ML of the SL stack that are coherently strained. The relaxation of the SL with increasing thickness corresponds therefore to the smaller redshift of 0.7 $\mathrm{cm}^{-1}$.

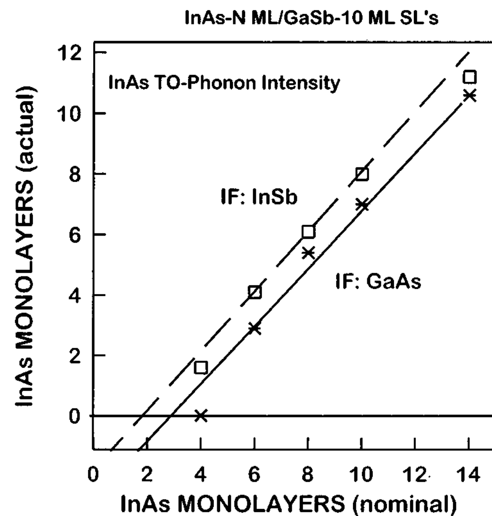


FIG. 18. Actual thickness of the InAs layers in $N/10$ SL's grown with either InSb-like IF's (squares) or GaAs-like IF's (crosses) determined by theoretical fits to the experimental reflectance spectra vs the nominal thickness.

The spectrally sharp feature in the GaSb TO-phonon band observed for the samples with GaAs-like IF bonds can be explained by a frequency shift of the GaSb TO phonon of the SL layers relative to the frequency of the TO mode in the GaSb buffer layer due to the strain relaxation of the SL's grown with GaAs-like IF's. The top part of these SL's is relaxed to a smaller in-plane lattice parameter, which induces the frequency shift of the GaSb TO phonon. This explanation is supported by the observation that the SL's grown with InSb-like IF's do not show this sharp feature, except for the sample with the thinnest InAs layers, which is known to be partially relaxed. The other SL's of this series are coherently strained.

Besides the information on the strain situation of the SL's obtained from the frequencies of the TO phonons, further insights can be gained by analyzing the mode intensities. In Fig. 18 the actual InAs layer thickness per SL period, determined by fitting the FIR reflectance spectra, is plotted versus the nominal InAs layer thickness given by the number of In-containing atomic planes. In SL's with InSb-like IF's bonds the nominal width of the InAs layers for each pair of samples is smaller by 1 ML compared to SL's with GaAs-like IF's. Surprisingly, the SL's with GaAs-like IF's show a less intense InAs TO phonon signal, and thus a smaller actual InAs layer thickness, than SL's with InSb-like IF's (see Fig. 18). For both types of IF's the actual InAs layer thickness varies linearly with the nominal InAs layer thickness with an extrapolated actual layer thickness of zero for a nominal thickness of 2–3 ML. For all $N/10$ SL samples with $N\geqslant 6$ the actual thickness of the InAs layers, which contribute to the TO phonon signal, is smaller than the nominal InAs layer thickness by the same amount. For the 4/10 GaSb SL's there is an even further reduction of the actual thickness compared to the value expected from the linear extrapolation of the data for $N\geqslant 6$. From the analysis of the HRXRD data

TABLE V. Results of the numerical evaluation of the FIR reflectance of the series of $N/10$ SL's grown with InSb-like interfaces.

| Nominal comp. InAs/GaSb (ML) | Evaluated thickness (ML) InAs | Phonon energies ($cm^{-1}$) InAs TO | GaSb TO |
|---|---|---|---|
| 4/10 | 1.6 | | 228 |
| 6/10 | 4.1 | 217.2 | 228 |
| 8/10 | 6.1 | 217.2 | 228 |
| 10/10 | 8.0 | 217.5 | 228 |
| 14/10 | 11.2 | 271.7 | 228 |

it is known that the difference between the nominal and the actual SL period is below 1 ML (see Sec. III, Table II). Therefore, we have to conclude that certain regions within the individual InAs layer do not contribute to the InAs TO phonon signal.

The same conclusion has been reached, based on IR absorption data, for InAs/AlSb quantum wells.[21,23] Recently, a possible explanation of this phenomenon has been given[22] on the basis of the assumption of a discontinuous strain distribution within the InAs layers in the vicinity of the IF's. A change of the lattice parameter in the planes facing the IF's results in a shift of the TO phonon frequency of the InAs layers adjacent to the IF's. Provided that this shift is comparable to the damping of the vibrational mode, the contribution to the reflectance spectrum from the TO phonon mode in these InAs layers adjacent to the IF's and that from the TO mode in the remainder of the InAs layer can cancel each other. A model of two oscillators spaced by about 5 $cm^{-1}$ (Ref. 22) interfering destructively in the reflectivity spectrum explains in particular the absence of any detectable InAs TO phonon signal in the reflectivity spectra of the 4/10 GaSb SL's (see Fig. 16).

A variation of the lattice parameter, and thus of the elastic strain, in the vicinity of the IF's, relative to the lattice spacing in the remainder of the layer, has been suggested by Hemstreet, Fong, and Nelson[4] based on theoretical calculations. These calculations predict in the case of GaAs-like IF bonds an increase of the interatomic spacing by 1.8% for the In-As backbonds of the IF. For InSb-like IF bonds a decrease of the length of these backbonds by 1.5% is predicted. These theoretical predictions give support to the above model of two oscillators with slightly different eigenfrequencies used to explain the absence of the InAs TO phonon signal for the 4/10 SL's.

## VI. SUMMARY AND CONCLUSIONS

We have studied the structural and vibrational properties of InAs/GaSb SL's grown by solid-source MBE on (100) GaAs substrates using strain-relaxed GaSb buffer layers. Two series of SL's with either InSb-like or GaAs-like IF's were prepared for nominal InAs layer thicknesses ranging from 4 to 14 ML while the GaSb layer thickness was kept constant at 10 ML. The intended formation of InSb-like or GaAs-like IF bonds was verified by Raman scattering from IF modes.

HRXRD studies including two-dimensional angular space maps allowed us to determine the average SL period and the average lattice parameter parallel and perpendicular to the growth direction. The SL's with InSb-like IF's were found to be coherently strained to the in-plane lattice parameter of the strain-relaxed GaSb buffer layer for InAs layer thicknesses ⩾6 ML. SL's with GaAs-like IF's showed a strain distribution within the SL stack with the first 10–20 SL periods being coherently strained but the remaining part of the SL stack showing an increasing degree of relaxation with increasing distance from the SL-buffer interface. The details of this strain distribution depend on the SL period. Bringing the GaAs-like IF's closer together by reducing the InAs layer width, and thus the SL period, was found to result in a decrease of the critical layer thickness for strain relaxation.

In view of the results of the present HRXRD analysis it is interesting to note that InAs/GaSb SL's grown on a GaSb buffer with InSb-like IF's are expected to be close to strain compensation because the larger lattice parameter of the InSb IF layers at least partially offsets the smaller lattice parameter of the InAs layers, depending on the SL period. For SL's with GaAs-like IF's, in contrast, the smaller lattice parameters of the GaAs IF layers and of the InAs layers add up to an average SL lattice parameter significantly smaller than that of the GaSb buffer layer. Thus, SL's with GaAs-like IF's are expected to be subjected to much higher tensile strains and the critical thickness of the SL stack for the onset of strain relaxation is expected to be much smaller than for SL's with InSb-like IF's, which is what has been observed in the present study.

Zone-folded LA phonon modes were observed up to the seventh order for SL's with InSb-like IF's and up to the fifth order for structures with GaAs-like IF bonds.[46] This difference in the maximum number of resolved zone-folded phonon modes indicates a higher crystalline perfection of the SL's with InSb-like IF's, which is in agreement with the HRXRD data. Taking the average SL periods obtained by HRXRD, the mode frequencies found for SL's with InSb-like IF's can be well reproduced by taking a SL sound velocity given by the weighted average over the sound velocities of bulk InAs and GaSb. SL's with GaAs-like IF's, in contrast, showed systematically higher mode frequencies, which indicates an increase in the SL sound velocity due to the Ga-As IF bonds.

From a quantitative analysis of FIR reflection spectra the individual layer thicknesses and the spatial extent of the GaAs-like IF mode were determined. The thicknesses of the InAs layers contributing to the InAs TO phonon signal were found to be smaller by 3–4 ML compared to the nominal values. This discrepancy has been explained by strained InAs regions adjacent to the IF's, which do not contribute to the bulklike InAs TO phonon signal but show a TO phonon frequency shifted slightly due to additional strain effects. The partial relaxation of the SL's grown with GaAs-like IF's becomes observable in the FIR spectra due to a blueshifting of the GaSb TO phonon. The frequency-shifted phonon mode induces a sharp resonance on top of the reststrahlen band of the GaSb buffer layer.

It has been shown that the present InAs/GaSb SL's exhibit much more intense band-to-band photoluminescence for structures with InSb-like IF's than for those with GaAs-like IF's.[54] This observation is fully consistent with the structural analysis of these SL's presented here. Further, for a given SL period also the effective SL band gap was found to

depend on the types of IF bonds. The strain relaxation of the SL stack grown with GaAs IF's induces a decrease of the in-plane lattice parameter with increasing thickness. This decrease results in a redshift of the effective band gap. In addition, the effect of the IF bonds formed on the strength of the IF dipoles, and thus on the band offset and the effective SL band gap, has to be taken into account.[54]

In conclusion, InAs/GaSb SL's with InSb-like and GaAs-like IF bonds, grown on (100) GaAs substrates by placing a thick strain-relaxed GaSb buffer layer between the SL stack and the substrate, have been studied by HRXRD, Raman spectroscopy, and FIR reflection spectroscopy. A detailed analysis of the structural properties of these SL's has been presented for both types of IF bonds. The SL's with InSb-like IF's showed superior structural properties and were found to be essentially coherently strained. SL's with GaAs-like IF's, in contrast, showed strain relaxation except for the first 10–20 SL periods closest to the GaSb buffer. Here, the strain profiles, deduced from simulations of the x-ray reflection profiles, were found to depend critically on the InAs layer thickness.

## ACKNOWLEDGMENTS

We would like to thank G. Bihlmann for valuable technical assistance in the MBE growth and F. Pohl for technical support of the HRXRD and Raman experiments. K. Schwarz is thanked for his support in the FIR reflection measurements. Valuable contributions by D. Behr to the Raman spectroscopic analysis are gratefully acknowledged.

## APPENDIX A

The experimental results of the HRXRD measurements are conveniently described in terms of the reciprocal lattice concept.[55,56] With respect to the broadening of diffraction peaks this approach has been successfully applied in powder diffractometry to single out the various sources of broadening.[57,58] Compared with powder diffractometry the experimental situation in HRXRD is much better defined and the additional information can be used to determine structural parameters orientation dependent. Thus averaged crystallite sizes, strains and tilts parallel and perpendicular to a growth surface can be discriminated.

The coordinate system we chose is defined by the incident wave vector $\mathbf{k}_0$ and the scattered wave vector $\mathbf{k}_H$, which define the scattering plane in reciprocal space and the scattering vector $\mathbf{q}=\mathbf{k}_H-\mathbf{k}_0$ lying in this plane. For convenience we define two vectors $\mathbf{k}_{00L}$ (perpendicular to the sample surface) and $\mathbf{k}_{HK0}$ (parallel to the sample surface). The components of the scattering vector $\mathbf{q}$ in the directions of $\mathbf{k}_{00L}$ and $\mathbf{k}_{HK0}$ are $q_{00L}$ and $q_{HK0}$, respectively.

A peak position given in terms of the angular space coordinates $\omega$ and $2\Theta$ then translates into reciprocal space coordinates by the relationships:

$$q_{00L}=(2/\lambda)\sin(2\Theta/2)\cos(\Theta-\omega), \quad \text{(A1)}$$

$$q_{hk0}=-(2/\lambda)\sin(2\Theta/2)\sin(\Theta-\omega), \quad \text{(A2)}$$

Here $2\Theta$ denotes the scattering angle given by $2\Theta=\Theta_0+\Theta_H$. Lattice parameters $a_\perp$ and $a_\parallel$ of a tetragonally distorted layer are calculated from peak positions in an $HKL$ space map using $a_\perp=L/q_{00L}$ and $a_\parallel=(H^2+K^2)^{1/2}/q_{hk0}$. The differential variation near the Bragg reflection $q_{HKL}=H_{HKL}$ follows from partial differentiation:

$$\delta q_{00L}=(1/\lambda)\cos(2\Theta-\omega)\,\delta 2\Theta + (2/\lambda)\sin(\Theta)\sin(\Theta-\omega)\,\delta\omega, \quad \text{(A3)}$$

$$\delta q_{HK0}=-(1/\lambda)\sin(2\Theta-\omega)\,\delta 2\Theta + (2/\lambda)\sin(\Theta)\cos(\Theta-\omega)\,\delta\omega. \quad \text{(A4)}$$

For an $\omega$ scan ($\delta 2\Theta=0$; $\delta\omega\neq 0$) we obtain

$$\delta q_{00L}=(2/\lambda)\sin(\Theta)\sin(\Theta-\omega)\,\delta\omega, \quad \text{(A3'a)}$$

$$\delta q_{HK0}=(2/\lambda)\sin(\Theta)\cos(\Theta-\omega)\,\delta\omega. \quad \text{(A4'a)}$$

For an $\Theta/2\Theta$ scan ($\delta 2\Theta\neq 0$; $\delta\omega=\delta\Theta\neq 0$) we obtain

$$\delta q_{00L}=(2/\lambda)\cos(\Theta)\cos(\Theta-\omega)\,\delta\omega, \quad \text{(A3''b)}$$

$$\delta q_{HK0}=-(2/\lambda)\cos(\Theta)\sin(\Theta-\omega)\,\delta\omega. \quad \text{(A4''b)}$$

The broadening of reflections in different measurement geometries can thus be translated into reciprocal space, where a decomposition of different contributions to the observed broadening of reciprocal lattice points (RELP's) can be accomplished. We have to consider the following broadening mechanisms:

(i) Tilting of an otherwise perfect crystal lattice around an axis results in a smearing out of those reciprocal lattice points not located on this axis. If we assume that the tilting occurs around several axes lying at random in a common plane [e.g., the (001) plane of the substrate], we end up with small reciprocal disks centered at the location of the former reciprocal lattice points. The extension of these disks on their appropriate sphere in reciprocal space is proportional to the amount of tilt $\Delta_M$ and the distance from the origin of the reciprocal lattice. Thus, in a diffraction experiment, we will encounter roughly the same reflection half-width (FWHM) while we scan, e.g., 002, 004, and 006 reflections by rotating the sample around the $\omega$ axis, keeping the detector at a fixed $2\theta$ position. The reflection broadening $\Delta\omega_M$ due to mosaicity tilts $\Delta_M$ will be best resolved in ''pure'' $\omega$ scans and is independent of the Bragg angle. In reciprocal space the appropriate broadening $\Delta q_M$ of $00L$ RELP's is

$$\Delta q_M=\Delta_M q_{00L}=\Delta\omega_M(2/\lambda)\sin\Theta. \quad \text{(A5)}$$

(ii) Reducing the number of reflecting lattice planes $(hkl)$ results in a corresponding broadening of all RELP's parallel to the $HKL$ direction in reciprocal space, the size of the RELP being proportional to the reciprocal of the number of reflecting lattice planes. Assuming that the average size $\langle t\rangle$ of coherently reflecting domains is reduced parallel to the (001) substrate plane, all reciprocal lattice points will be smeared out into disks parallel to the $HK0$ reciprocal lattice plane. The size $\Delta q_{CS}$ of these disks only depends on $1/\langle t_{HKL}\rangle$ and is independent of their respective distance from the origin of the reciprocal lattice. If we perform the same diffraction experiment as described in (i), we will find now

that reflections closer to the origin (e.g., 002) have a larger FWHM than have those further away from the origin (e.g., 006). The reflection broadening $\Delta\omega_{CS}$ due to crystallite size effects thus varies with the Bragg angle and, most important, $\omega$ scans and $\Theta/2\Theta$ scans yield the crystallite size distribution parallel ($\Delta q_{CS,HK0}$) and perpendicular ($\Delta q_{CS,00L}$) to the samples (001) plane, respectively,

$$\Delta q_{CS} = 1/\langle t_{HKL}\rangle, \tag{A6}$$

$$\Delta q_{CS,HK0} = 1/\langle t_{HK0}\rangle = \Delta\omega_{CS,HK0}(2/\lambda)\sin\Theta, \tag{A6a}$$

$$\Delta q_{CS,00L} = 1/\langle t_{00L}\rangle = \Delta\omega_{CS,00L}(2/\lambda)\cos\Theta, \tag{A6b}$$

(iii) Inhomogeneous strain $\langle\epsilon\rangle$ perpendicular to a lattice plane $(hkl)$ will broaden all RELP's parallel to the $HKL$ direction in reciprocal space to an extent depending on the amount of strain and the direction cosine between the strain direction and the direction of the scattering vector pointing toward the RELP. With a pseudomorphic film grown on a cubic (001) plane a variation of the strain within the film parallel to the growth surface is not possible; here, only a strain variation $\langle\epsilon_{00L}\rangle$ perpendicular to the (001) plane has to be considered. This will not hold for (partially) relaxed films where $\langle\epsilon_{HK0}\rangle$ will in general be finite. However, with a cubic (001) surface orientation only asymmetric and ''in-plane'' reflections ($q_{HK0}\neq 0$) will be affected by such a variation of the strain, whereas symmetric $00L$ reflections ($q_{HK0}=0$) will merely be broadened by strain components parallel to [001], i.e., $\langle\epsilon_{00L}\rangle$. The reflection broadening $\Delta q_{ST,00L}$ due to a variation of the strain $\langle\epsilon_{00L}\rangle$ can thus be measured in $\Theta/2\Theta$ scans and depends on the Bragg angle:

$$\Delta q_{ST,00L} = \langle\epsilon_{00L}\rangle q_{00L}/2 = \Delta\omega_{ST,00L}(1/2\lambda)\cos\Theta. \tag{A7}$$

With more than one cause for reflection broadening present, the combined effect depends on the individual shape of the diffraction profiles. There is ample literature on this subject.[57,60] The peak profiles measured in this study showed perfect or near Gaussian shape, which led us to assume Gaussian profiles for the individual profiles too. The first of the two fundamental equations for the evaluation of our FWHM measurements obtained in this way is well known in powder diffractometry where the evaluation of $\Theta/2\Theta$ scans of $00L$ reflections uses

$$\begin{aligned}(\Delta q_{00L})^2 &= (\Delta q_{CS,00L})^2 + (\Delta q_{ST,00L})^2\\ &= (1/\langle t_{00L}\rangle)^2 + (\langle\epsilon_{00L}\rangle q_{00L}/2)^2\end{aligned} \tag{A8}$$

and the evaluation of $\omega$ scans of $00L$ reflections uses

$$\begin{aligned}(\Delta q_{HK0})^2 &= (\Delta q_{CS,HK0})^2 + (\Delta_M)^2\\ &= (1/\langle t_{HK0}\rangle)^2 + (\Delta_M q_{00L})^2.\end{aligned} \tag{A9}$$

A plot of $\Delta q^2$ against $q^2$ with data obtained via $\Theta/2\Theta$ scans at $00L$ reflections yields the mean crystallite dimensions perpendicular ($\langle t_{00L}\rangle$) to the (001) surface from the intercept $b_{00L}$ with the ordinate: $(\langle t_{00L}\rangle)^2 = 1/b_{00L}$. From the slope $m_{00L}$ the lattice distortions $\langle\varepsilon_{00L}\rangle$ parallel to [001] are obtained using $(\langle\varepsilon_{00L}\rangle)^2 = 4m_{00L}$. In the same way the crystallite dimensions parallel to the surface $\langle t_{00L}\rangle$ and the maximal mosaicity tilts $\Delta_M$ are obtained with data from $\omega$ scans of $00L$ reflections using $(\langle t_{HK0}\rangle)^2 = 1/b_{HK0}$ and $(\Delta_M)^2 = m_{HK0}$.

## APPENDIX B

The experimental spectra of the FIR reflectance were fitted by theoretical reflectivity spectra obtained by calculating the transfer matrix of the propagation of the electromagnetic radiation in the whole stratified medium.[49] In order to best model the reflectance spectra of the investigated samples, not only the reflectance of the SL but also that of the buffer layers and of the substrate have to be taken into account. Generally, at near-normal incidence, the propagation of electromagnetic radiation through a medium $i$ of thickness $d_i$ and dielectric function

$$\varepsilon_i(\omega) = \varepsilon_{\infty,i}\frac{\omega_{LO,i}^2 - \omega^2 - i\omega\Gamma_i}{\omega_{TO,i}^2 - \omega^2 - i\omega\Gamma_i} \tag{B1}$$

is given by[49]

$$\begin{pmatrix}E_i^+\\ E_i^-\end{pmatrix} = \begin{pmatrix}e^{-2\pi\sqrt{\varepsilon_i}d_i\omega} & \phi 0\\ 0\,\phi & e^{+2\pi\sqrt{\varepsilon_i}d_i\omega}\end{pmatrix}\begin{pmatrix}E_{if}^+\\ E_{if}^-\end{pmatrix} = L_i\begin{pmatrix}E_{if}^+\\ E_{if}^-\end{pmatrix}, \tag{B2}$$

where $E_i^+$ ($E_i^-$) is the forward (backward) component of the electric field at the beginning (subscript 0) and at the end (subscript $f$) of the medium, described by the layer matrix $L_i$. Here $\varepsilon_{\infty,i}$ is the high-frequency dielectric constant of the medium, $\omega_{TO,i}$ and $\omega_{LO,i}$ are the transverse and longitudinal optical phonon frequency and $\Gamma_i$ is the phonon damping factor. In most cases medium 0 will be vacuum (air) and medium $f$ the substrate. The propagation of the electromagnetic field through the interface between two media $i$ and $j$ is described by the interface matrix $I_{ij}$ defined in the following equation:

$$\begin{pmatrix}E_i^+\\ E_i^-\end{pmatrix} = \frac{1}{t_{ij}}\begin{pmatrix}1 & r_{ij}\\ r_{ij} & 1\end{pmatrix}\begin{pmatrix}E_j^+\\ E_j^-\end{pmatrix} = I_{ij}\begin{pmatrix}E_i^+\\ E_i^-\end{pmatrix}. \tag{B3}$$

In the equation above, $r_{ij}$ and $t_{ij}$ are the complex Fresnel coefficients,

$$r_{ij} = \frac{\sqrt{\varepsilon_i} - \sqrt{\varepsilon_j}}{\sqrt{\varepsilon_i} + \sqrt{\varepsilon_j}}, \tag{B4a}$$

$$t_{ij} = \frac{2\sqrt{\varepsilon_i}}{\sqrt{\varepsilon_i} + \sqrt{\varepsilon_j}}, \tag{B4b}$$

The propagation of light from medium 0 to medium $f$ through a stratified medium composed of $n$ layers is then described by the transfer matrix

$$M = I_{01}\times L_1 \times I_{12}\times\cdots\times I_{nf}\times L_f = \frac{1}{t_{0f}}\begin{pmatrix}A & B\\ C & D\end{pmatrix}, \tag{B5}$$

where

$$t_{0f} = t_{01}\times t_{12}\times\cdots t_{nf} \tag{B6}$$

so that

$$\begin{pmatrix} E_0^+ \\ E_0^- \end{pmatrix} = M \begin{pmatrix} E_f^+ \\ E_f^- \end{pmatrix}. \tag{B7}$$

The reflectivity of the multilayer then is given by

$$R = \frac{|A|^2}{|C|^2} \tag{B8}$$

and the transmittance is given by

$$T = \frac{1}{|C|^2}. \tag{B9}$$

The dielectric function of the InAs/GaSb SL's was described in the framework of the effective medium approximation,

$$\varepsilon_{\text{SL}} = \frac{\Sigma_j d_j \varepsilon_j}{\Sigma_j d_j}, \tag{B10}$$

where $j=1,2,...$ defines the layers $j$ composing one SL period. To take into account the GaAs-like bonds at the interface of the SL, one SL period has been modeled by the following sequence of atomic layers:

$$(\text{InAs})_{N'}(\text{GaAs-IF})_{N''}(\text{GaSb})_{M'}(\text{GaAs-IF})_{M''}. \tag{B11}$$

This fitting procedure allowed us to determine the energy of the phonons confined in each layer of the SL or localized at the interface, as well as the actual thickness of each layer and of the interface region. In the case of GaAs-like IF layers, the damping factor $\Gamma$ has also been determined. Phonon damping factors in the range 2–3 $\text{cm}^{-1}$ were used for the InAs and GaSb phonons in the SL. The parameters of the materials composing the buffer layers and the substrate were taken from Ref. 35.

---

*Present address: SDL Inc., San Jose, CA 95134-1365.

[1] L. L. Chang, N. Kawai, G. A. Sai-Halasz, R. Ludeke, and L. Esaki, Appl. Phys. Lett. **35**, 939 (1979).

[2] D. L. Smith and C. Mailhiot, J. Appl. Phys. **62**, 2545 (1987).

[3] R. H. Miles, D. H. Chow, Y.-H. Zhang, P. D. Brewer, and R. G. Wilson, Appl. Phys. Lett. **66**, 1921 (1995).

[4] L. A. Hemstreet, C. Y. Fong, and J. S. Nelson, J. Vac. Sci. Technol. B **11**, 1693 (1993).

[5] D. M. Symons, M. Lakrimi, R. J. Warburton, R. J. Nicholas, N. J. Mason, P. J. Walker, and M. I. Eremets, Semicond. Sci. Technol. **9**, 118 (1994); D. M. Symons, M. Lakrimi, M. van der Burgt, T. A. Vaughan, R. J. Nicholas, N. J. Mason, and P. J. Walker, Phys. Rev. B **51**, 1729 (1995).

[6] J. R. Meyer, C. A. Hoffman, B. V. Shanabrook, B. R. Bennett, R. J. Wagner, J. R. Waterman, and E. R. Youngdale, in *Proceedings of the 22nd International Conference on the Physics of Semiconductors, Vancouver, Canada, 1994*, edited by D. J. Lockwood (World Scientific, Singapore, 1995), p. 783.

[7] J. R. Waterman, B. V. Shanabrook, R. J. Wagner, M. J. Yang, J. L. Davis, and J. P. Omaggio, Semicond. Sci. Technol. **8**, S106 (1993).

[8] P. Fewster, Appl. Surf. Sci. **50**, 9 (1991).

[9] P. van der Sluis, J. Phys. D **26**, A188 (1993); P. van der Sluis, J. Appl. Cryst. **27**, 1025 (1994).

[10] E. Koppensteiner, T. W. Ryan, M. Heuken, and J. Söllner, J. Phys. D **26**, A35 (1993).

[11] B. R. Bennett, B. V. Shanabrook, R. J. Wagner, J. L. Davis, and J. R. Waterman, Appl. Phys. Lett. **63**, 949 (1993).

[12] J. Spitzer, H. D. Fuchs, P. Etchegoin, M. Ilg, M. Cardona, B. Brar, and H. Kroemer, Appl. Phys. Lett. **62**, 2274 (1993).

[13] See, e.g., B. Jusserand and M. Cardona, in *Light Scattering in Solids V*, edited by M. Cardona and G. Güntherodt (Springer, Berlin, 1989), p. 49.

[14] A. Fasolino, E. Molinari, and J. C. Maan, Phys. Rev. B **33**, 8889 (1986).

[15] A. Fasolino, E. Molinari, and J. C. Maan, Phys. Rev. B **39**, 3923 (1989); Superlattices Microstruct. **3**, 117 (1987).

[16] Y. Liu and B. J. Inkson, Semicond. Sci. Technol. **4**, 1167 (1989).

[17] D. Kechrakos and J. C. Inkson, Semicond. Sci. Technol. **6**, 155 (1991).

[18] D. Berdekas and G. Kanellis, Phys. Rev. B **43**, 9976 (1991).

[19] M. Yano, H. Furuse, Y. Iwai, K. Yoh, and M. Inoue, J. Cryst. Growth **127**, 807 (1993).

[20] M. J. Yang, R. J. Wagner, B. V. Shanabrook, W. J. Moore, and J. R. Waterman, C. H. Yang, and M. Fatemi, Appl. Phys. Lett. **63**, 3434 (1993).

[21] F. Fuchs, J. Schmitz, K. Schwarz, J. Wagner, J. D. Ralston, and P. Koidl, Appl. Phys. Lett. **65**, 2060 (1994).

[22] C. Gadaleta, G. Scamarcio, F. Fuchs, and J. Schmitz, J. Appl. Phys. **78**, 5642 (1995).

[23] M. J. Yang, R. J. Wagner, B. V. Shanabrook, W. J. Moore, J. R. Waterman, M. E. Twigg, and M. Fatemi, Appl. Phys. Lett. **61**, 583 (1992).

[24] J. Shen, S. Y. Ren, and J. D. Dow, Phys. Rev. B **46**, 6938 (1992).

[25] J. Schmitz, J. Wagner, F. Fuchs, N. Herres, P. Koidl, and J. D. Ralston, J. Cryst. Growth **150**, 858 (1995).

[26] Here we define 1 ML as a bilayer of group III and group V atoms, which has a thickness of twice the interatomic distance along the (100) direction or one-half of the lattice parameter. The nominal thickness of the InAs and GaSb layers within one SL period is given by the number of atomic planes containing group III atoms.

[27] W. Bartels, J. Vac. Sci. Technol. B **1**, 338 (1983).

[28] W. L. Bond, Acta Crystallogr. **13**, 814 (1960).

[29] S. Groβwig, K.-H. Jäckel, R. Kittner, B. Dietrich, and U. Schellenberger, Cryst. Res. Technol. **20**, 1093 (1985).

[30] R. Zaus, J. Appl. Cryst. **26**, 801 (1993).

[31] N. Herres, G. Bender, and G. Neumann, Appl. Surf. Sci. **50**, 97 (1991).

[32] WIN-HRXRD Version 2, Siemens AG, München 1995.

[33] D. Behr, J. Wagner, J. Schmitz, N. Herres, J. D. Ralston, and P. Koidl, Appl. Phys. Lett. **65**, 2972 (1994).

[34] A. McL. Mathieson and A. W. Stevenson, Acta Crystallogr. A **51**, 391 (1995).

[35] *Semiconductors. Physics of Group IV Elements and III-V Compounds*, edited by O. Madelung, Landolt-Börnstein, New Series, Group III, Vol. 17, Pt. a (Springer-Verlag, Berlin, 1982).

[36] M. Krieger, H. Sigg, N. Herres, K. Bachem, and K. Köhler, Appl. Phys. Lett. **66**, 682 (1995).

[37] J. C. Brice, in *Properties of Gallium Arsenide*, 2nd ed., EMIS Datareviews Series No. 2 (INSPEC, IEE, London, 1990), Chap. 1, p. 18.

[38] N. S. Takahashi and M. Matsuura, in *Properties of Lattice-*

*matched and Strained Indium Gallium Arsenide*, EMIS Datareviews Series (INSPEC, IEE, London, 1993), Chap. 2.2, p. 41.

[39] B. R. Bennett, B. V. Shanabrook, R. J. Wagner, J. L. Davis, J. R. Waterman, and M. E. Twigg, Solid-State Electron. **37**, 733 (1994).

[40] J. Spitzer, A. Höpner, M. Kuball, M. Cardona, B. Jenichen, H. Neuroth, B. Brar, and H. Kroemer, J. Appl. Phys. **77**, 811 (1995).

[41] J. L. Lazzari, C. Fouillant, P. Grunberg, J. L. Leclercq, A. Jouillié, and C. Schiller, J. Cryst. Growth **130**, 96 (1993).

[42] R. N. Kyutt, L. M. Sorokin, T.-S. Argunova, and S. S. Ruvimov, Phys. Solid State **36**, 1473 (1994); Fiz. Tverd. Tela (St. Petersburg) **36**, 2700 (1994).

[43] S. G. Lyapin, P. C. Klipstein, N. J. Mason, and P. J. Walker, Superlattices Microstruct. **15**, 499 (1994), Phys. Rev. Lett. **74**, 3285 (1995).

[44] B. V. Shanabrook, B. R. Bennett, and R. J. Wagner, Phys. Rev. B **48**, 17 172 (1993).

[45] B. Jusserand, P. Voisin, M. Voos, L. L. Chang, E. E. Mendez, and L. Esaki, Appl. Phys. Lett. **46**, 678 (1985).

[46] J. Wagner, J. Schmitz, N. Herres, J. D. Ralston, and P. Koidl, Appl. Phys. Lett. **66**, 3498 (1995).

[47] B. Jusserand, F. Alexandre, J. Dubard, and D. Paquet, Phys. Rev. B **33**, 2897 (1986).

[48] J. R. Drabble and A. J. Brammer, Proc. Phys. Soc. **91**, 959 (1967).

[49] M. Born and E. Wolf, *Principles of Optics* (Pergamon, New York, 1975).

[50] B. V. Shanabrook and B. R. Bennett, Phys. Rev. B **50**, 1695 (1994).

[51] R. Carle, N. Saint-Criq, J. B. Renucci, M. B. Renucci, and A. Zwick, Phys. Rev. **22**, 4804 (1980).

[52] F. Cerdeira, C. J. Buchenauer, F. H. Pollak, and M. Cardona, Phys. Rev. B **5**, 580 (1972).

[53] E. Anastassakis, A. Cantarero, and M. Cardona, Phys. Rev. B **41**, 7529 (1990).

[54] F. Fuchs, J. Schmitz, N. Herres, J. Wagner, J. D. Ralston, and P. Koidl, in *Proceedings of the 7th International Conference on Narrow Gap Semiconductors, Santa Fe, 1995*, IOP Conf. Proc. No. 144, edited by J. L. Reno (Institute of Physics, Bristol, 1995), p. 219; F. Fuchs, N. Herres, J. Schmitz, K. M. Pavlov, J. Wagner, P. Koidl, and J. H. Roslund, Proc. SPIE **2554**, 70 (1995).

[55] L. V. Azároff, *Elements of X-ray Crystallography* (McGraw-Hill, New York, 1968).

[56] *International Tables for Crystallography, Vol. B: Reciprocal Space*, edited by U. Shmueli (Kluwer Academic, Dordrecht, 1993).

[57] H. P. Klug and L. E. Alexander, *X-ray Diffraction Procedures* 2nd ed. (Wiley, New York, 1974).

[58] R. C. Reynolds Jr., in *Reviews in Mineralogy*, Modern Powder Diffraction Vol. 20, edited by D. L. Bish and J. E. Post (The Mineralogical Society of America, Washington, D.C., 1989), p. 1.

[59] T. S. Argunova, R. N. Kyutt, M. P. Scheglov, and N. N. Faleev, J. Phys. D **28**, A212 (1995).

[60] A. Taylor, *X-ray Metallography* (McGraw-Hill, New York, 1961).